



# UEx-L-Eddies: decadal and global long-lived mesoscale eddy trajectories with coincident air–sea CO<sub>2</sub> fluxes and environmental conditions

Daniel J. Ford<sup>1</sup>, Jamie D. Shutler<sup>1</sup>, Katy L. Sheen<sup>1</sup>, Gavin H. Tilstone<sup>2</sup>, and Vassilis Kitidis<sup>2</sup>

<sup>1</sup>Centre for Geography and Environmental Sciences (CGES), University of Exeter, Penryn, UK

<sup>2</sup>Plymouth Marine Laboratory, Plymouth, UK

**Correspondence:** Daniel J. Ford (d.ford@exeter.ac.uk)

Received: 1 August 2025 – Discussion started: 14 August 2025

Revised: 19 December 2025 – Accepted: 26 January 2026 – Published: 5 February 2026

**Abstract.** Mesoscale eddies are prevalent features within the global ocean that modify the physical, chemical and biological properties as they move and evolve. These modifications can alter the air–sea exchange of CO<sub>2</sub>, and therefore these features may be hotspots for enhanced or reduced CO<sub>2</sub> uptake compared to the surrounding environment. The understanding of the global and regional effect of mesoscale eddies on ocean CO<sub>2</sub> uptake is limited and largely based on single eddies or small regional subsets. Here, we provide a global dataset of 5996 long lived eddies (lifetimes greater than a year) with corresponding air–sea CO<sub>2</sub> fluxes between 1993 to 2022 all tracked using a Lagrangian approach. The trajectories comprise 3244 anticyclonic (“warm core”) and 2752 cyclonic (“cold core”) eddies and the dataset provides the environmental conditions, including the CO<sub>2</sub> fluxes, within and outside each eddy. The dataset refines a previous regional methodology with a focus on climate quality environmental parameters and uses a global neural network for estimating the fugacity of CO<sub>2</sub> in seawater ( $f\text{CO}_{2(\text{sw})}$ ) along with a comprehensive air–sea CO<sub>2</sub> flux uncertainty budget. These refinements provide a robust foundation for studying the modulation of air–sea CO<sub>2</sub> fluxes by mesoscale eddies. As an example use of the dataset, we investigate the role of mesoscale eddies in modifying the global and regional air–sea CO<sub>2</sub> fluxes, by comparing the eddy driven air–sea CO<sub>2</sub> flux to that of the surrounding environment. We find that globally, long-lived anticyclonic eddies enhanced the CO<sub>2</sub> sink by  $4.5 \pm 2.8\%$  (95 % confidence), while long-lived cyclonic eddies reduce the CO<sub>2</sub> sink by  $0.7 \pm 2.6\%$ . Collectively, the long-lived mesoscale eddies indicate an enhancement of the ocean CO<sub>2</sub> sink by  $2.7 \pm 1.1 \text{ Tg C yr}^{-1}$ . Propagating the air–sea CO<sub>2</sub> flux uncertainties was found to be a key component needed to fully understand apparent differences between previous regional and global studies. The long-lived mesoscale eddies (UEx-L-Eddies) dataset is available on Zenodo at <https://doi.org/10.5281/ZENODO.16355763> (Ford et al., 2025).

## 1 Introduction

Mesoscale eddies are known to affect the physical, chemical and biological properties of the oceans (Dufois et al., 2016; Frenger et al., 2013; Laxenaire et al., 2019; Li et al., 2025; Nencioli et al., 2018; Orselli et al., 2019a, b; Pezzi et al., 2021). These rotating bodies of water have radii on the order 100 km, lifetimes from a few days to multiple years, and can transit ocean basins transporting distinct water masses within them (Chelton et al., 2011; Pegliasco et al.,

2022b). Eddies generally fall into two categories; (1) anticyclonic and (2) cyclonic. Anticyclonic eddies are associated with high pressure centres, clockwise rotation in the Northern Hemisphere (or anticlockwise in the Southern Hemisphere), warmer sea surface temperatures (SST), and a depression of isopycnals (and downwelling of water within the eddy core). Whereas cyclonic eddies are generally the opposite; low pressure centres, anticlockwise rotation in the Northern Hemisphere (or clockwise in the Southern Hemisphere), cooler SSTs, and an elevation of isopycnals (and up-

welling in the eddy core). During their lifetimes, these eddies can alter the air-sea  $\text{CO}_2$  exchange through their modification of the ocean and atmospheric properties. As the  $\text{CO}_2$  solubility in seawater is highly temperature sensitive, the  $f\text{CO}_{2(\text{sw})}$  in anticyclonic eddies could theoretically be elevated and therefore the features may act as a weaker  $\text{CO}_2$  sink or stronger  $\text{CO}_2$  source compared to the surrounding environment. Conversely the opposite may be true for cyclonic eddies, with reduced  $f\text{CO}_{2(\text{sw})}$ , and increased capacity to act as a stronger ocean  $\text{CO}_2$  sink. Mesoscale eddies are complex dynamic features however, and these generalisations may not always apply as their response will always be dependent upon the ocean basin conditions. Where the eddy formed, how it evolves and interacts with ocean water and the atmosphere, also needs to be considered. For example, Chen et al. (2007) identified a cyclonic eddy acting as a weaker  $\text{CO}_2$  sink compared to the surrounding environment due to upwelling of  $\text{CO}_2$  and nutrients within the eddy core. Orselli et al. (2019b) showed six anticyclonic Agulhas eddies that were acting as a stronger  $\text{CO}_2$  sink (than the surrounding water) during Austral winter. Pezzi et al. (2021) identified an anticyclonic eddy acting as a strong  $\text{CO}_2$  source in the Southwestern Atlantic. Whereas, through using a biogeochemical model, Song et al. (2016) suggested that these eddy modifications may have seasonal differences, whereby anticyclonic (cyclonic) eddies acted as stronger (weaker)  $\text{CO}_2$  sinks in summer, but stronger (weaker) sources in winter.

Despite the abundance of mesoscale eddies, previous studies generally investigate single eddies (Chen et al., 2007; Jones et al., 2017; Pezzi et al., 2021) or a regional subset of eddies (Ford et al., 2023; Orselli et al., 2019b; Song et al., 2016) and their effect on the air-sea  $\text{CO}_2$  flux. Thus, the global cumulative effect of all types of eddies on the air-sea  $\text{CO}_2$  flux is still under investigation. Ford et al. (2023), used a Lagrangian tracking approach and suggested that long-lived (lifetimes greater than one year) mesoscale eddies enhanced the air-sea  $\text{CO}_2$  flux in the South Atlantic Ocean by  $\sim 0.05 \text{ Tg C yr}^{-1}$  ( $\sim 0.08\%$ ). Guo and Timmermans (2024) used a spatial and timeseries decomposition to extract the mesoscale flow impact on the air-sea  $\text{CO}_2$  fluxes globally, and estimate a small integrated effect of  $0.72 \text{ Tg C yr}^{-1}$  (compared to global ocean uptake of  $\sim 2.9 \text{ Pg C yr}^{-1}$ ). However, this result may include mesoscale signals not related to mesoscale eddies (Guo and Timmermans, 2024). Li et al. (2025), using a method that tracked individual eddies similar to Ford et al. (2023), showed that mesoscale eddies within the Kuroshio and Gulf Stream western boundary currents could enhance the  $\text{CO}_2$  sink by  $28.34 \pm 9.41 \text{ Tg C yr}^{-1}$ .

In this paper we produce a global dataset of long lived (defined as lifetimes greater than one year) mesoscale eddies ( $N = 5996$ ; radii  $> 30 \text{ km}$ ) and their associated air-sea  $\text{CO}_2$  fluxes tracked in a Lagrangian mode between 1993 and 2022. The methodology refines the approach described in Ford et al. (2023), using a global neural network approach and published tools which are also used to generate one ocean carbon

sink dataset submission to the annual Global Carbon Budget assessments (Friedlingstein et al., 2025). Following recommendations for global ocean carbon assessments (Shutler et al., 2024) we prioritise the use of climate quality satellite data records (Embry et al., 2024; Sathyendranath et al., 2019) within the analysis. The uncertainties on the air-sea  $\text{CO}_2$  fluxes are systematically assessed following the work of Ford et al. (2024a). These refinements provide a robust foundation to studying the modulation of air-sea  $\text{CO}_2$  flux by mesoscale eddies, with an uncertainty budget. We demonstrate the use of the global dataset to assess regional and global air-sea  $\text{CO}_2$  fluxes of long-lived eddies and to estimate their net impact on  $\text{CO}_2$  uptake of the ocean.

## 2 Methods

Figure 1 shows a schematic of the implementation of the methodology within this study to estimate the air-sea  $\text{CO}_2$  flux within mesoscale eddies.

### 2.1 Satellite and reanalysis data

The importance of prioritising the use of climate data records to study long time series and the ocean carbon sink was highlighted in Shutler et al. (2024). We used the European Space Agency's climate change initiative (CCI) climate data records SST-CCI (v3;  $\sim 4 \text{ km}$ ; 1993 to 2022) for SST (Embry et al., 2024; Good and Embry, 2024) and the Ocean Colour CCI (OC-CCI) for the chlorophyll *a* (chl *a*) concentrations (v6;  $\sim 4 \text{ km}$ ; 1997 to 2022; Sathyendranath et al., 2019, 2023), with their respective per observation uncertainties (Table 1). The CCI-SST was bias corrected for a cool bias with respect to global SST drifters, representative of SST at 20 cm ( $\sim 0.05 \text{ K}$ ; Embry, 2023; Embry et al., 2024), which is used to provide an accurate estimation of  $f\text{CO}_{2(\text{sw})}$  (in Sect. 2.3), and for the air-sea  $\text{CO}_2$  flux calculation (in Sect. 2.4).

We were unable to use the sea surface salinity (SSS) CCI climate data record for our application due to the 8 d temporal resolution of these data. We therefore used the Copernicus Marine Service GLORYS12V1 ocean reanalysis product for SSS ( $\sim 9 \text{ km}$ ; 1993 to 2022; CMEMS, 2021; Jean-Michel et al., 2021), and the ocean mixed layer depth (MLD) as no climate data record is available for MLD. No climate data record is available for wind speed, therefore the Cross-Calibrated Multi-Platform (CCMP) wind speed dataset (6-hourly;  $\sim 25 \text{ km}$ ; 1993 to 2022) was chosen (Mears et al., 2022; Remote Sensing Systems et al., 2022) which is often used for ocean carbon assessments (Ford et al., 2024a).

### 2.2 Eddy trajectories Atlas

The satellite altimetry based Mesoscale Eddy Product (version META3.2) as described in Pegliasco et al. (2022a, b),

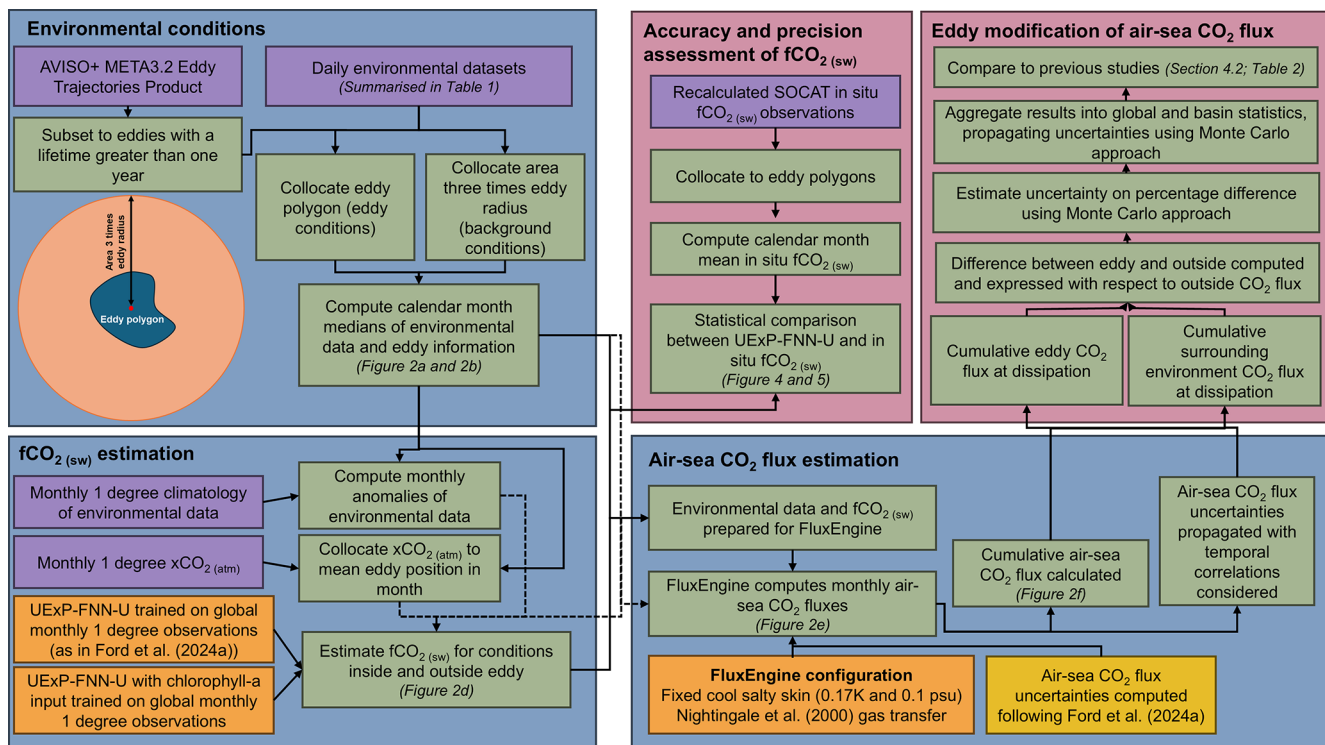


**Figure 1.** Schematic showing the processing steps to estimate the air-sea  $\text{CO}_2$  flux within long lived eddies (Blue box background). The pink background boxes indicate the analysis completed to evaluate the accuracy and precision of the dataset. In figure acronyms are: fugacity of  $\text{CO}_2$  in seawater ( $f\text{CO}_2(\text{sw})$ ), atmospheric dry mixing ratio of  $\text{CO}_2$  ( $x\text{CO}_2(\text{atm})$ ) and University of Exeter feed forward neural network with uncertainties (UEExP-FNN-U).

and distributed by the Archiving, Validation, and Interpretation of Oceanographic Satellite data (AVISO), was used to identify the trajectories of mesoscale eddies between 1993 and 2022. We extracted the eddy trajectories globally, that had a lifetime greater than one year, which gave 3244 anticyclonic eddies and 2752 cyclonic eddies for further analysis. The focus on these long-lived eddies was due to their presence likely exhibiting a larger influence on the air-sea  $\text{CO}_2$  flux (e.g. Smith et al., 2023). Additionally, the selection was due to computational limitations in running the analysis for the extensive set of shorter lived eddies within the dataset. We are working to extend the analysis to shorter lived eddies but currently the focus remains on long lived eddies.

For each eddy trajectory, a daily position was provided along with a polygon shape that estimates the eddy shape and size from the altimetry-based data which can not overlap with land. These eddy polygons were used to extract a daily timeseries of the environmental data described in Sect. 2.1, where the daily conditions within the eddy were calculated (mean, median, standard deviation, interquartile range, maximum number of available data points, number of valid data points). This was repeated for the area surrounding the eddy, where we consider the ‘area outside’ to be a circle centred on the eddy but with three times the mean radius of the eddy and the area inside the eddy polygon itself removed. The chosen

radii (of three times the mean radius) was used as Ford et al. (2023) showed that the results of their study were consistent when using a “surrounding area criterion” between two and five radii.

Daily timeseries of conditions within and surrounding the eddy, were then converted to a monthly median timeseries using the daily median values. The daily median was chosen to reduce the impact of any potential outliers caused by any limited data coverage due to cloud cover in the chl  $a$  record. The daily median and mean were generally consistent for the SST, SSS, MLD and wind speed fields as these are spatially complete fields.

### 2.3 $f\text{CO}_2(\text{sw})$ neural network (UEExP-FNN-U) and uncertainty

The monthly  $f\text{CO}_2(\text{sw})$  and air-sea gas fluxes were estimated using the methods and tools of the University of Exeter Physics Feed Forward neural network with uncertainties (UEExP-FNN-U) which are routinely used to generate ocean sink data for the annual Global Carbon Budget assessments (Friedlingstein et al., 2025), and described in Ford et al. (2024a). The UEExP-FNN-U approach estimates the  $f\text{CO}_2(\text{sw})$  based on in situ data that is considered representative of the subskin layer ( $\sim 0.2$  m water depth), which al-

**Table 1.** Summary of the environmental datasets and in situ observations collocated with the long lived mesoscale eddies.

Parameter	Units	Dataset	Temporal resolution	Spatial resolution	Reference
Sea surface temperature	Kelvin	ESA CCI-SST v3.0	Daily	~ 5 km (0.05°)	Embry et al. (2024), Good and Embry (2024)
Sea surface salinity	Psu	CMEMS GLORYS12V1	Daily	~ 9 km (0.08°)	CMEMS (2021), Jean-Michel et al. (2021)
Mixed layer depth	m	CMEMS GLORYS12V1	Daily	~ 9 km (0.08°)	CMEMS (2021), Jean-Michel et al. (2021)
Chlorophyll <i>a</i>	mg m <sup>-3</sup>	OC-CCI v6	Daily	4 km	Sathyendranath et al. (2019, 2023)
Wind speed	m s <sup>-1</sup>	CCMP v3.1	6 hourly	~ 25 km (0.25°)	Mears et al. (2022), Remote Sensing Systems et al. (2022)
Sea level pressure	hPa	ERA5	Monthly	~ 25 km (0.25°)	Hersbach et al. (2019, 2020)
<i>x</i> CO <sub>2</sub> (atm)	ppm	NOAA-GML	Monthly	~ 100 km (1°)	Lan et al. (2023)
<i>f</i> CO <sub>2</sub> (sw)	μatm	Recalculated SOCAT	Individual cruise observations	n/a	Bakker et al. (2016) Ford et al. (2024d)

n/a stands for not applicable.

lows for an accurate air sea CO<sub>2</sub> flux calculation (Woolf et al., 2016; Sect. 2.4). The methods used are consistent with those in Ford et al. (2024a), so only a summary of the method is provided here. The UExP-FNN-U is a two-step self-organising map (SOM) feed forward neural network (FNN) setup. The SOM splits the global ocean into 16 regions with a similar *f*CO<sub>2</sub>(sw), SST, SSS and MLD seasonal cycles. A FNN ensemble (10 FNNs for each region) was then trained with in situ monthly 1° *f*CO<sub>2</sub>(sw) observations from the Surface Ocean CO<sub>2</sub> Atlas (SOCAT; Bakker et al., 2016) that have been recalculated to a consistent temperature and depth dataset (Ford et al., 2024d). The monthly 1° predictor variables of SST, SSS, MLD and the atmospheric dry mixing ratio of CO<sub>2</sub> (*x*CO<sub>2</sub>(atm)), and anomalies of each with respect to a long term monthly climatology were collocated to the in situ *f*CO<sub>2</sub>(sw). The FNNs consists of an input layer with nodes equal to the number of input predictors, a hidden layer with a varying number of nodes depending on a pretraining step and an output layer with a single node. The training data were split into a 95 % training and validation dataset, and a 5 % independent test randomly for each month ensuring the independent data were not clustered in one region. The UExP-FNN-U *f*CO<sub>2</sub>(sw) estimates are then typically used to estimate the global ocean CO<sub>2</sub> sink as described in Ford et al. (2024a).

To estimate the *f*CO<sub>2</sub>(sw) for each eddy the monthly median timeseries of the SST, SSS, MLD were provided to the UExP-FNN-U. The *x*CO<sub>2</sub>(atm) was calculated from the National Oceanic and Atmospheric Administration Global Monitoring Laboratory (NOAA-GML) monthly 1° fields (Lan et al., 2023) that were used within the neural network training. These *x*CO<sub>2</sub>(atm) fields were produced by calculating the monthly average of the *x*CO<sub>2</sub>(atm) for each latitude (~ 2.5° spacing), which were then interpolated to 1° and replicated for each 1° longitude. A distance weighted mean of the nearest four pixels taken at the mean (centre) position of each eddy was used to estimate the monthly *x*CO<sub>2</sub>(atm). Anomalies in SST, SSS, MLD and *x*CO<sub>2</sub>(atm) were calculated with respect to a 1° monthly climatology.

The uncertainties in the *f*CO<sub>2</sub>(sw) were calculated as described in Ford et al. (2024a). The *f*CO<sub>2</sub>(sw) uncertainty has three components: (1) the network uncertainty estimated as the two standard deviation of the 10 neural network ensemble, (2) the parameter uncertainty was the propagated input parameter uncertainties and was estimated using a lookup table and (3) the evaluation uncertainty which was the evaluation with respect to the SOCAT observations (Bakker et al., 2016). All three components are combined in quadrature, assuming they are independent and uncorrelated (Taylor, 1997), to provide a total uncertainty (considered 95 %

confidence). The uncertainty components were calculated for each  $f\text{CO}_{2(\text{sw})}$  estimate.

Additionally, a second version of the neural network was run. This version included chl  $a$  (and the chl  $a$  anomaly) as a predictor and was used to produce a second estimate of  $f\text{CO}_{2(\text{sw})}$ . Ford et al. (2022a) highlighted that the inclusion of more representative biological parameters improved the regional estimation of  $f\text{CO}_{2(\text{sw})}$  in the South Atlantic Ocean. Therefore, this additional neural network output was generated using the same software used to create the UExP-FNN-U estimate of  $f\text{CO}_{2(\text{sw})}$  (Ford et al., 2024c) just with the added chl  $a$  predictor. However, we note the limitation of this second  $f\text{CO}_{2(\text{sw})}$  estimate that uses chl  $a$ . This dependency on optically derived remote sensing data (ie the chl  $a$  data) means that it was limited to producing estimates after October 1997 (as routine ocean colour observations are not available before this date) and it could not provide estimates during polar winter due to missing daily chl  $a$  data (as the low light levels inhibit optical retrievals).

The neural network estimated  $f\text{CO}_{2(\text{sw})}$  were compared to recalculated SOCAT observations (Ford et al., 2024d; Goddijn-Murphy et al., 2015) within eddies to assess the accuracy and precision of the estimates. The individual cruise SOCAT observations are gridded (to monthly  $1^\circ$ ) to provide the training and independent test data to the UExP-FNN-U, and therefore these  $f\text{CO}_{2(\text{sw})}$  observations are not strictly independent. For each eddy trajectory, the ungridded SOCAT observations were collocated with the daily eddy polygon. The daily SOCAT observations that fell within the eddy were then aggregated into monthly mean  $f\text{CO}_{2(\text{sw})}$ , which could be compared to the neural network monthly  $f\text{CO}_{2(\text{sw})}$ . We calculated a series of statistics including the bias, root mean square difference (RMSD), slope and intercept of a Type II linear regression to characterise the differences between the neural network outputs and monthly mean SOCAT  $f\text{CO}_{2(\text{sw})}$ . A Type II linear regression was used as uncertainties are presented within both the in situ and neural network  $f\text{CO}_{2(\text{sw})}$  (Laws, 1997; York et al., 2004). As in Ford et al. (2021) weighted variants of these statistics were also calculated to capture the uncertainties in both sets of data (neural network output and the SOCAT in situ data), assuming a SOCAT  $f\text{CO}_{2(\text{sw})}$  uncertainty of  $5 \mu\text{atm}$  (Bakker et al., 2016) and the calculated neural network total  $f\text{CO}_{2(\text{sw})}$  uncertainty.

#### 2.4 Air-sea $\text{CO}_2$ flux calculations and uncertainties

The  $\text{CO}_2$  flux calculations were performed using Flux-Engine v4.0.9.1 (Holding et al., 2019; Shutler et al., 2016), using the “rapid” transport approximation (Woolf et al., 2016), at monthly time steps. The evidence continues to grow supporting the calculation of air-sea  $\text{CO}_2$  fluxes with consideration of the vertical temperature gradients, which is supported by theoretical (Woolf et al., 2016), observation based (Dong et al., 2022b; Shutler et al., 2020; Watson et al., 2020),

modelling (Bellenger et al., 2023), and recently two in situ studies (Dong et al., 2024; Ford et al., 2024b). Therefore, the air-sea  $\text{CO}_2$  fluxes were calculated using a bulk formulation that allows for the vertical temperature gradients to be captured. The calculations are consistent with the methods used to create the UExP-FNN-U dataset that is submitted to the annual Global Carbon Budget assessments (Friedlingstein et al., 2025), except here a simplified approach to determine the skin SST value is used.

The air sea  $\text{CO}_2$  flux ( $F$ ) was calculated as:

$$F = k_{600} (Sc/600)^{-0.5} (\alpha_{\text{subskin}} f\text{CO}_{2(\text{sw,subskin})} - \alpha_{\text{skin}} f\text{CO}_{2(\text{atm})}) \quad (1)$$

where  $k$  is the gas transfer velocity estimated from the monthly wind speeds and the Nightingale et al. (2000) gas transfer parameterisation.  $\alpha_{\text{subskin}}$  and  $\alpha_{\text{skin}}$  are the solubility of  $\text{CO}_2$  at the base, and top of the mass boundary layer respectively, and were calculated as a function of SST and SSS (Weiss, 1974).  $\alpha_{\text{subskin}}$  was calculated from the bias corrected CCI-SST SST and the CMEMS SSS.  $\alpha_{\text{skin}}$  was calculated with the same datasets, but with a fixed cool ( $-0.17 \text{ K}$ ) (Donlon et al., 1999) and salty ( $+0.1 \text{ psu}$ ) skin effect. We used a fixed cool skin here, instead of the dynamic cool skin approach (that uses COARE 3.5; Fairall et al., 1996) as used within the UExP-FNN-U Global Carbon Budget submission due to the computation overhead needed to extract the additional environmental fields required for the calculations. This simplified approach has only a small effect on the global scale (Dong et al., 2022b), and therefore we do not see it as a limitation.  $f\text{CO}_{2(\text{atm})}$  was estimated for the NOAA-GML  $x\text{CO}_{2(\text{atm})}$ , ERA5 sea level pressure (Hersbach et al., 2019) and the CCI-SST with a cool salty skin following Dickson et al. (2007).  $f\text{CO}_{2(\text{sw,subskin})}$  was provided by the neural network  $f\text{CO}_{2(\text{sw})}$ . The ERA5 sea level pressure was retrieved from monthly  $0.25^\circ$  fields, using a distance weighted mean of the 4 closest observations to the mean monthly eddy position. None of the eddies considered were under sea ice (as the eddy detection data and algorithm cannot track in areas of ice), and therefore the term “1 – ice” which is generally included within Eq. (1) (to linearly scale the gas fluxes with sea ice concentration) has not been included.

The air-sea  $\text{CO}_2$  flux uncertainties were calculated following the methods in Ford et al. (2024a), and consistent literature values for the uncertainties in the wind speed ( $1.9 \text{ m s}^{-1}$ ; 95 % confidence; Mears et al., 2022), salinity ( $0.2 \text{ psu}$ ; 95 % confidence; Jean-Michel et al., 2021),  $x\text{CO}_{2(\text{atm})}$  ( $0.4 \mu\text{atm}$ ; 95 % confidence; Lan et al., 2023) and gas transfer parameterisation (20 %; 95 % confidence; Woolf et al., 2019). The SST uncertainty was extracted from the daily CCI-SST dataset and were converted to monthly uncertainties assuming a 5 d temporal correlation (Ford et al., 2024a). The uncertainties were calculated at the 95 % confidence (or the  $2\sigma$ ).

The monthly mean daily flux of  $\text{CO}_2$  ( $\text{g C m}^{-2} \text{ d}^{-1}$ ) was multiplied by the number of days and the mean area of

the eddy as provided by the eddy trajectories, in the respective month. The fluxes (Tg C per month) were then added cumulatively to retrieve the net cumulative CO<sub>2</sub> flux for each eddy (Tg C). Collating the combined uncertainties requires careful consideration of their temporal correlations. Some uncertainties will be temporally decorrelated, and others have temporal correlations. We used the assumptions made in Ford et al. (2024a), that the SST, SSS, wind speed,  $x\text{CO}_2(\text{atm})$  and  $f\text{CO}_2(\text{sw})$ , and components dependent on these uncertainties, are temporally uncorrelated and are therefore propagated assuming they are independent (Taylor, 1997). Whereas, the remaining uncertainties that stem from the Schmidt number, solubilities and gas transfer parameterisation algorithm uncertainties are assumed temporally correlated and therefore are summed (Ford et al., 2024a). The air-sea CO<sub>2</sub> flux calculations and uncertainty estimates were computed for the two variants of  $f\text{CO}_2(\text{sw})$ . The computations were also applied separately for the eddy and the area outside the eddy, assuming the same area coverage of the eddy for both calculations (i.e. allowing the cumulative fluxes to be compared for the same area coverage).

## 2.5 Modification of air-sea CO<sub>2</sub> fluxes due to the existence of the eddy

As shown in Ford et al. (2023), the air-sea CO<sub>2</sub> flux into an eddy can be considered as two components: (1) the flux that would occur without the presence of the eddy and (2) the mesoscale modification of the flux through both oceanic and atmospheric effects of the eddy presence. The flux that would occur without the eddy being present can be estimated using the conditions that are driving the air-sea CO<sub>2</sub> flux in the environment surrounding the eddy. This reference flux can be removed from the air-sea CO<sub>2</sub> flux calculated for within the eddy to indicate the mesoscale modification of the flux due to the existence of the eddy, which was converted to a percentage change with respect to the surrounding environment CO<sub>2</sub> flux, following Ford et al. (2023).

The eddy modification of the air-sea CO<sub>2</sub> flux was calculated for each individual eddy, and then the median percentage modification was estimated for global and regional subsets, due to the lower sensitivity to outliers. We repeat the percentage change calculations in a Monte Carlo uncertainty propagation approach to evaluate the full extent of the uncertainties, whereby the eddy modification flux was perturbed within their uncertainties (95 %) 1000 times independently (i.e., assuming the individual eddy flux modification uncertainties are uncorrelated). The two standard deviation value of the resulting ensemble was taken as the 95 % confidence on the median percentage change for the global or regional subsets due to the uncertainties.

## 3 Results

### 3.1 Geographical distribution of mesoscale eddy cumulative air-sea CO<sub>2</sub> flux

In total 5996 eddies were tracked and their air-sea CO<sub>2</sub> flux estimated, which comprised 3244 anticyclonic and 2752 cyclonic eddies between 1993 and 2022 (Fig. 2). The geographical distribution of the cumulative air-sea CO<sub>2</sub> flux into both eddy types generally followed the global distribution of air-sea CO<sub>2</sub> fluxes. The temperate regions showed eddies with strong CO<sub>2</sub> sink characteristics over their lifetimes, whereas eddies in the subtropical showed weaker CO<sub>2</sub> sinks, or even CO<sub>2</sub> sources. Regionally the Indian Ocean showed stronger CO<sub>2</sub> sinks associated with anticyclonic eddies when compared to the Atlantic and Pacific Oceans (Fig. 2a). The South Pacific showed anticyclonic eddies acting as weaker CO<sub>2</sub> sinks compared to the North Pacific and had more eddies acting as CO<sub>2</sub> sources. Notable regions where cyclonic eddies were acting as strong CO<sub>2</sub> sinks are within the Indian Ocean, and Northwestern Atlantic Ocean (Fig. 2b). Cyclonic eddies in the South Pacific tended to act more as CO<sub>2</sub> sources than sinks (Fig. 2b). The Southern Ocean showed the anticyclonic and cyclonic eddies acting as either weak CO<sub>2</sub> sinks or weak CO<sub>2</sub> sources (Fig. 2).

### 3.2 Example eddy trajectory

Figure 3 shows an example of an eddy trajectory in the North Pacific Ocean that was selected due to the ~3 year lifetime, that highlights the seasonality and variability of the environmental data, the  $f\text{CO}_2(\text{sw})$  and associated air-sea CO<sub>2</sub> fluxes with the uncertainties shown. Over the three years the eddy moves around a relatively small region within the subpolar region (Fig. 3c). Within the eddy, an expected SST seasonal cycle was present (Fig. 3a), along with an interannual variability within the SSS timeseries (Fig. 3b). The estimated  $f\text{CO}_2(\text{sw})$  also highlighted a clear seasonal cycle with higher  $f\text{CO}_2(\text{sw})$  in the winter months, and lower  $f\text{CO}_2(\text{sw})$  in the summer (Fig. 3d). The eddy exhibited a period of strong CO<sub>2</sub> outgassing during winter, followed by a small CO<sub>2</sub> sink within the summer months (Fig. 3e). When cumulatively summed, the air-sea CO<sub>2</sub> fluxes indicate that the eddy outgassed CO<sub>2</sub> over its lifetime, but clearly this outgassing was not year-round (Fig. 3f). The example eddy illustrates the available data that could be used to evaluate the driving mechanism that are affecting the  $f\text{CO}_2(\text{sw})$  and air-sea CO<sub>2</sub> fluxes over the eddy's lifetime.

### 3.3 UExP-FNN-U $f\text{CO}_2(\text{sw})$ compared to SOCAT observations within eddies

The UExP-FNN-U was trained on a global dataset of  $f\text{CO}_2(\text{sw})$  and so it is important to assess its performance within eddies providing some level of confidence that the eddy variability is being correctly captured. The within eddy

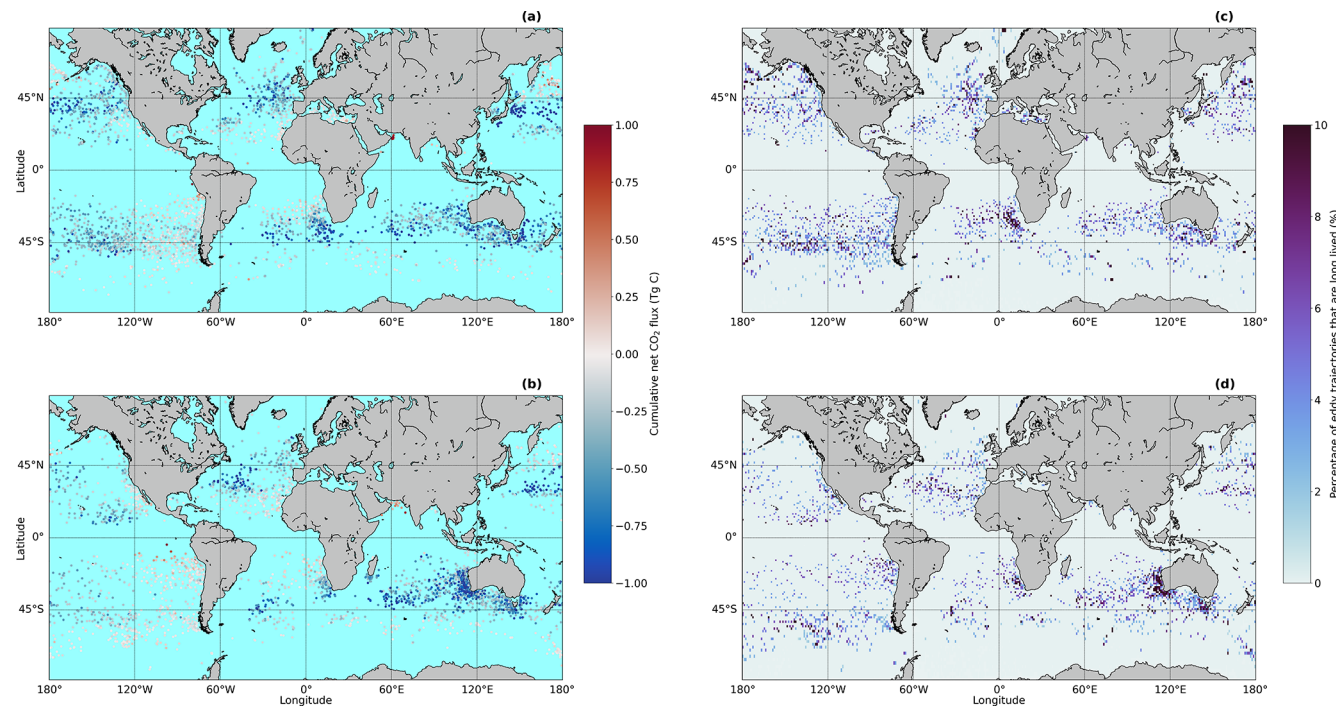


**Figure 2.** (a) The cumulative air-sea  $\text{CO}_2$  flux into the anticyclonic eddies where the scatter points are plotted at the formation location of each eddy. (b) Same as (a) but for cyclonic eddies. (c) The percentage of long lived anticyclonic eddy trajectories compared to all eddy trajectories that form in  $1^\circ$  by  $1^\circ$  regions. (d) Same as (c) but for cyclonic eddies. Basemap from Natural Earth v4.0.0 (<https://www.naturalearthdata.com/>, last access: 2 February 2025). Figure S1 shows the equivalent of (a) and (b) in  $\text{Tg C d}^{-1}$  to remove the differences in eddy lifetime.

accuracy and precision estimates between the SOCAT in situ observations and the UExP-FNN-U  $f\text{CO}_{2(\text{sw})}$  showed good performance (Fig. 4) similar to the results for the global scale in Ford et al. (2024a) (weighted bias =  $-0.18 \mu\text{atm}$ ,  $\text{RMSD} = 20.65$ ,  $N = 18\,226$  monthly  $1^\circ$  regions). For anticyclonic eddies, we observed a smaller weighted  $\text{RMSD}$  (precision) of  $19.15 \mu\text{atm}$  ( $N = 2082$  monthly matches; Fig. 4a). For cyclonic eddies we observed a lower  $\text{RMSD}$  of  $16.49 \mu\text{atm}$  ( $N = 1376$ ; Fig. 4d). Both eddy types showed small weighted biases (accuracy) and therefore we consider the UExP-FNN-U generated  $f\text{CO}_{2(\text{sw})}$  within eddies to sufficiently represent the eddy  $f\text{CO}_{2(\text{sw})}$ . The differences between the within-eddy UExP-FNN-U  $f\text{CO}_{2(\text{sw})}$  and in situ SOCAT observations did not indicate regional biases, but did show a spatial weighting to the Northern Hemisphere where more in situ  $f\text{CO}_{2(\text{sw})}$  are made (Bakker et al., 2016; Fig. 4c and f).

Seasonally separating the collocated within eddy in situ observations shows that the UExP-FNN-U tended to show a small weighted bias (accuracy) and smaller  $\text{RMSD}$  (precision) during winter and autumn (Fig. 5a, b, g and h) compared to spring and summer (Fig. 5c–f). Although winter and autumn tended to have lower collocations between in situ SOCAT observations and the UExP-FNN-U  $f\text{CO}_{2(\text{sw})}$  (Fig. 5). These seasonal comparisons further strengthen the

accuracy and precision of the UExP-FNN-U  $f\text{CO}_{2(\text{sw})}$  and indicates no large seasonal biases. Figure 4b and e shows that the uncertainties calculated for the  $f\text{CO}_{2(\text{sw})}$  were able to sufficiently represent the differences to the SOCAT observations. Thereby providing validity to the  $f\text{CO}_{2(\text{sw})}$  contribution to the air-sea  $\text{CO}_2$  flux uncertainty budgets.

#### 3.4 Uncertainty in the mesoscale eddy cumulative air-sea $\text{CO}_2$ flux

Two exemplar eddies, eddy A with a lifetime of 12 months and eddy B with a lifetime of 42 months, are shown in Fig. 6. These were selected to highlight the differences in the relative and absolute contributions of each uncertainty component to the total uncertainty, and how these can change over time for eddies of differing lifetimes. The absolute uncertainty magnitudes for eddy B were larger than eddy A (Fig. 6b, and d), but the relative contributions of each component showed similarities.

For both eddies at the end of their life, the  $f\text{CO}_{2(\text{sw})}$  component was the dominant source to the uncertainty for the whole lifetime, followed by the gas transfer parameterisation uncertainty. For eddy A, wind speed was the next largest contributor to the uncertainties, whereas for the eddy B, the solubility component uncertainties were larger than the wind speed uncertainty.

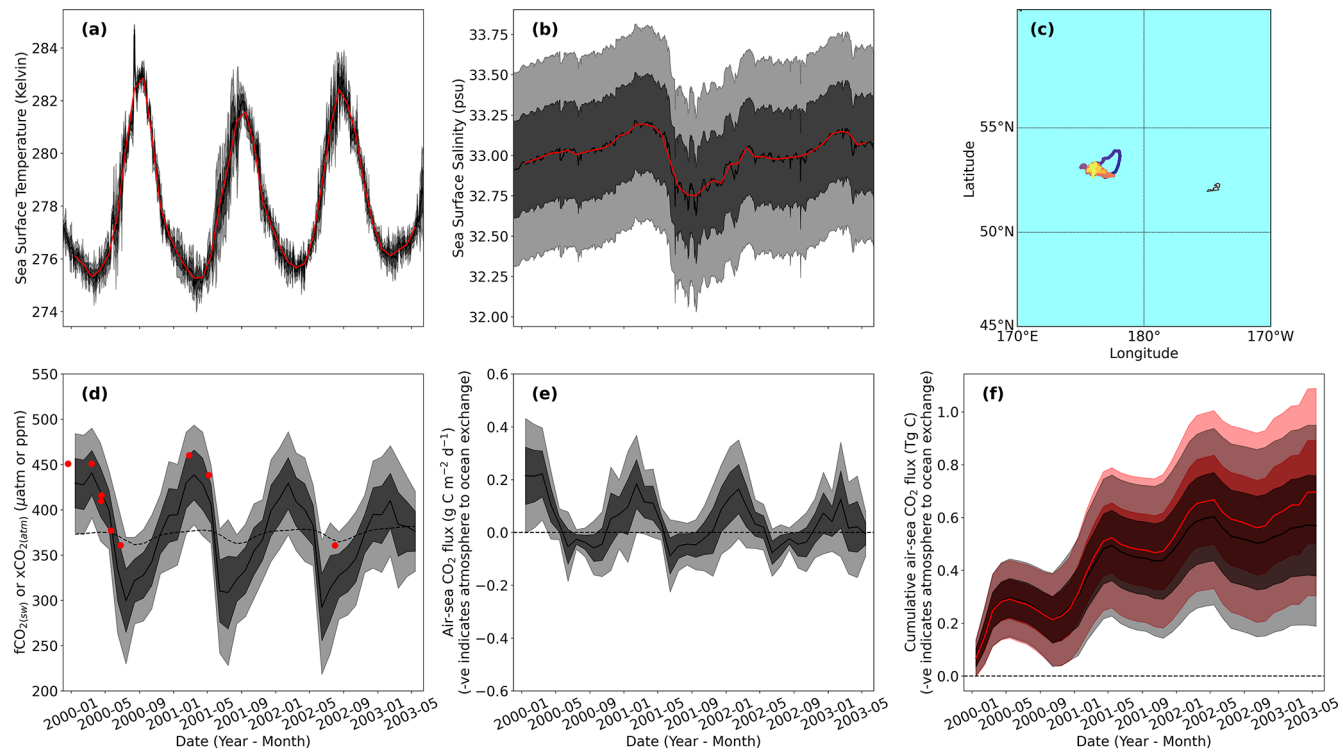


**Figure 3.** Exemplar eddy trajectory (eddy 194465) in the North Pacific Ocean with calculated air-sea CO<sub>2</sub> fluxes **(a)** Sea surface temperature (SST) for the example eddy's lifetime. Black line is the daily SST, where dark grey and light grey shading indicates the  $1\sigma$  ( $\sim 67\%$  confidence) and  $2\sigma$  ( $\sim 95\%$  confidence) uncertainties. Red line is the median monthly SST. **(b)** Same as **(a)** for sea surface salinity. **(c)** Geographical eddy trajectory, where colour indicates the age of eddy (blue is eddy formation and yellow is eddy dissipation). **(d)** Monthly timeseries of fugacity of CO<sub>2</sub> in seawater ( $f\text{CO}_2(\text{sw})$ ; solid line) and dry mixing ratio of CO<sub>2</sub> in the atmosphere ( $x\text{CO}_2(\text{atm})$ ; dashed line) for the eddy. Dark grey and light grey shading indicates the  $1\sigma$  ( $\sim 67\%$  confidence) and  $2\sigma$  ( $\sim 95\%$  confidence) uncertainties on the  $f\text{CO}_2(\text{sw})$ . Red dots indicate  $f\text{CO}_2(\text{sw})$  in situ observations from the Surface Ocean CO<sub>2</sub> Atlas within the eddy. **(e)** Same as **(d)** but for the air-sea CO<sub>2</sub> flux where a positive flux means CO<sub>2</sub> outgassing. Dashed black line indicates an air-sea CO<sub>2</sub> flux of 0. **(f)** Same as **(d)** but for the cumulative air-sea CO<sub>2</sub> flux. Red line and banding indicate the cumulative air-sea CO<sub>2</sub> flux for the surrounding environment.

Throughout both eddy lifetimes the dominant uncertainty contributions changed. For eddy A, at formation showed that the wind speed and solubility components were larger contributors than the gas transfer uncertainty until four months after formation (Fig. 6b). Within eddy B, the wind speed was a larger contributor than the solubility components until 12 months after formation, at which time the solubility component becomes a larger contributor (Fig. 6d). Uncertainties due to the Schmidt number and  $f\text{CO}_2(\text{atm})$  terms were a small contribution to the uncertainty in both eddies.

### 3.5 Global and regional mesoscale modifications of the air-sea CO<sub>2</sub> flux

An example application of the dataset was to assess the modification of the cumulative air-sea CO<sub>2</sub> flux by individual eddies at their dissipation. The analysis indicated that individual eddies could enhance (negative percentage changes) or suppress (positive percentage changes) the CO<sub>2</sub> sink (Fig. 7). Both anticyclonic (Fig. 7a) and cyclonic eddies (Fig. 7b) showed individual eddies that were either enhancing or sup-

pressing the air-sea CO<sub>2</sub> flux. Regional signatures in the air-sea CO<sub>2</sub> flux modification were apparent, for example anticyclonic eddies in the South Pacific and Southern Ocean had a greater tendency to enhance the CO<sub>2</sub> sink, whereas in the Indian Ocean there was not a discernible tendency. Cyclonic eddies in the Southern Ocean indicated a larger suppression of the CO<sub>2</sub> sink than for example the North Pacific.

Considering all the eddies studied and the calculated uncertainties, anticyclonic eddies were identified to enhance the cumulative CO<sub>2</sub> flux, where these eddies acted as stronger CO<sub>2</sub> sink (weaker CO<sub>2</sub> source) by  $4.5 \pm 2.8\%$  (95 % confidence). Cyclonic eddies indicated a slight suppression of the cumulative air-sea CO<sub>2</sub> flux by  $0.7 \pm 2.6\%$ , acting overall to weaken the CO<sub>2</sub> sinks (or as stronger CO<sub>2</sub> sources). Here we note, at the 95 % confidence the cumulative CO<sub>2</sub> sink enhancement by anticyclonic eddies was significantly different from 0 (i.e. the confidence interval did not include 0) when uncertainties were accounted for, but this was not significantly different from 0 for cyclonic eddies.

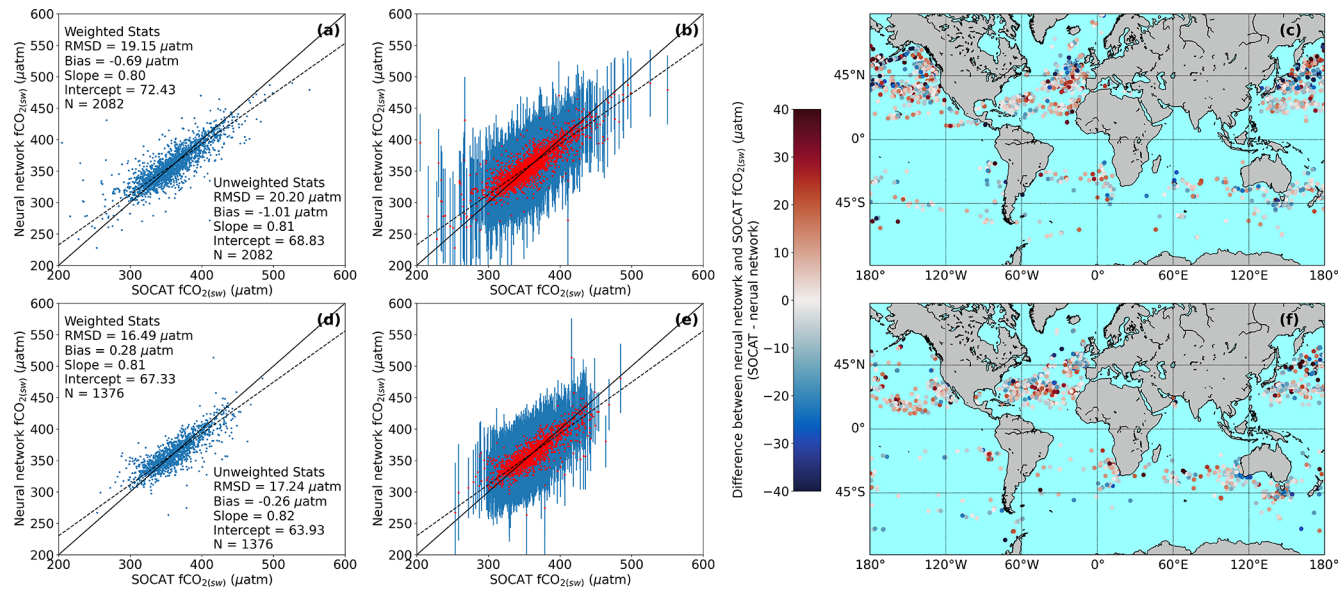


**Figure 4.** (a) Comparison of the UExP-FNN-U  $f\text{CO}_2\text{(sw)}$  to in situ SOCAT observations within anticyclonic eddies. Solid black line is the 1 : 1. Dashed line is the Type II linear regression. In text statistics are root mean square difference (RMSD), bias, slope and intercept of a Type II linear regression and number of matches ( $N$ ). (b) Same as (a) but showing the uncertainty on the  $f\text{CO}_2\text{(sw)}$  ( $2\sigma$ ; 95 % confidence) as errorbars for anticyclonic eddies. (c) Difference between UExP-FNN-U  $f\text{CO}_2\text{(sw)}$  to in situ SOCAT observations within anticyclonic eddies plotted as spatial residuals. (d–f) Same as (a)–(c) but for cyclonic eddies.

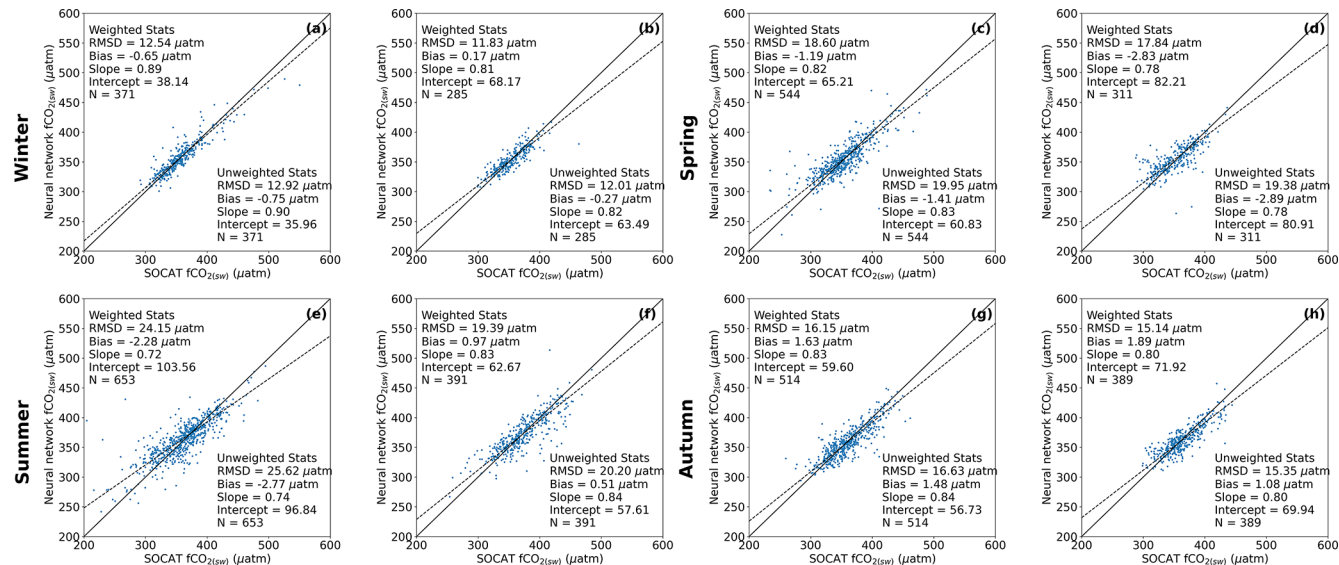


**Figure 5.** (a) Comparison of the UExP-FNN-U  $f\text{CO}_2\text{(sw)}$  to in situ SOCAT observations within anticyclonic eddies during winter. Solid black line is the 1 : 1. Dashed line is the Type II linear regression. In text statistics are root mean square difference (RMSD), bias, slope and intercept of a Type II linear regression and number of matches ( $N$ ). (b) Same as (a) but for cyclonic eddies in the winter. (c, d) same as (a) and (b) for spring. (e, f) Same as (a) and (b) for summer. (g, h) Same as (a) and (b) for autumn.

The regional differences can be emphasised by considering median eddy modifications within different regional subsets (Fig. 8) instead of globally (Fig. 8c and d). The eddy modification of  $\text{CO}_2$  fluxes within the regions showed differing magnitudes that fall within different significance bands when the uncertainties are accounted for. For example, the

Southern Ocean shows an anticyclonic enhancement of the  $\text{CO}_2$  sink of  $5.7 \pm 5.0\%$  (significant at 95 % confidence), with cyclonic eddies suppressing the  $\text{CO}_2$  sink by  $2.5 \pm 4.6\%$ . In the North Pacific, we find similar results where anticyclonic eddies enhance by  $5.6 \pm 5.2\%$ , and cyclonic eddies suppress by  $1.7 \pm 7.4\%$ . Consistent results were found for the South

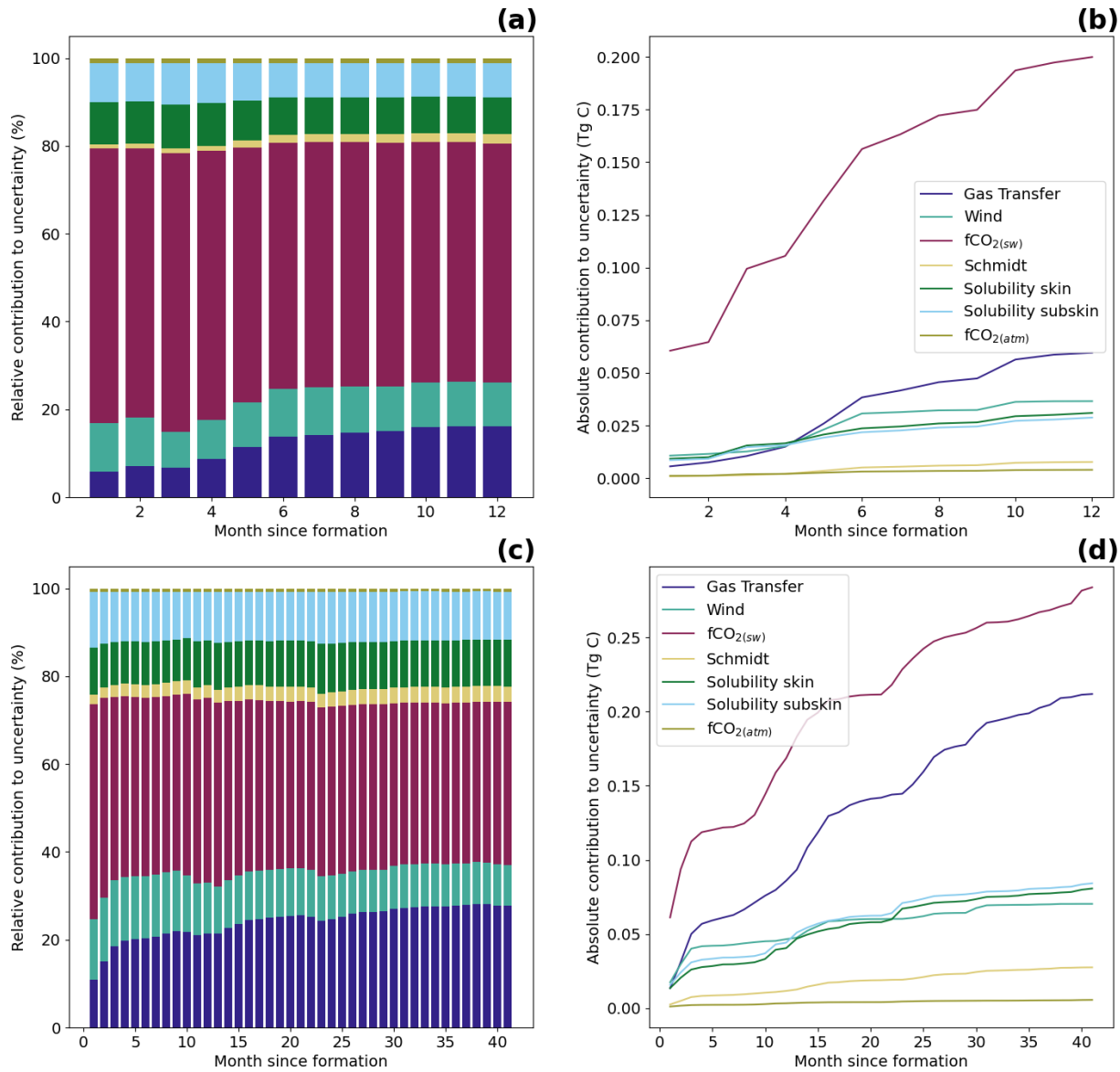


**Figure 6.** (a) The total cumulative air-sea  $\text{CO}_2$  flux uncertainty ( $2\sigma$ ) for an exemplar anticyclonic eddy, eddy A, (1 year lifetime; eddy 496) split into the relative contributions for the individual components. (b) The total air-sea  $\text{CO}_2$  flux uncertainty in absolute terms. Legend in (b) corresponds to colours in (a). (c, d) Same as (a) and (b) but for eddy B, an anticyclonic eddy (42 months lifetime; eddy 194465). Note different  $x$  axis limits for (a) and (b) compared to (c) and (d).

Pacific but noting the cyclonic eddies showed a larger uncertainty interval of  $11.5\%$ . The South Atlantic Ocean showed the anticyclonic enhancement of the sink by  $0.3 \pm 15.0\%$  and cyclonic eddies appear to enhance the  $\text{CO}_2$  sink by  $0.7 \pm 13.7\%$ . The uncertainty intervals on these are however the largest of any region, likely due to the lowest number of eddies considered.

## 4 Discussion

### 4.1 Mesoscale eddy air-sea $\text{CO}_2$ fluxes and uncertainties

The mesoscale eddy air-sea  $\text{CO}_2$  fluxes provide both the  $\text{CO}_2$  fluxes for each month with uncertainties and the corresponding environmental data (i.e. SST, SSS) within and outside of each eddy (Fig. 3). These data allow a range of analyses to be conducted, for example, in this study, we show how the mesoscale modification of the air-sea  $\text{CO}_2$  flux can be determined from these data regionally (Figs. 7 and 8) or could be

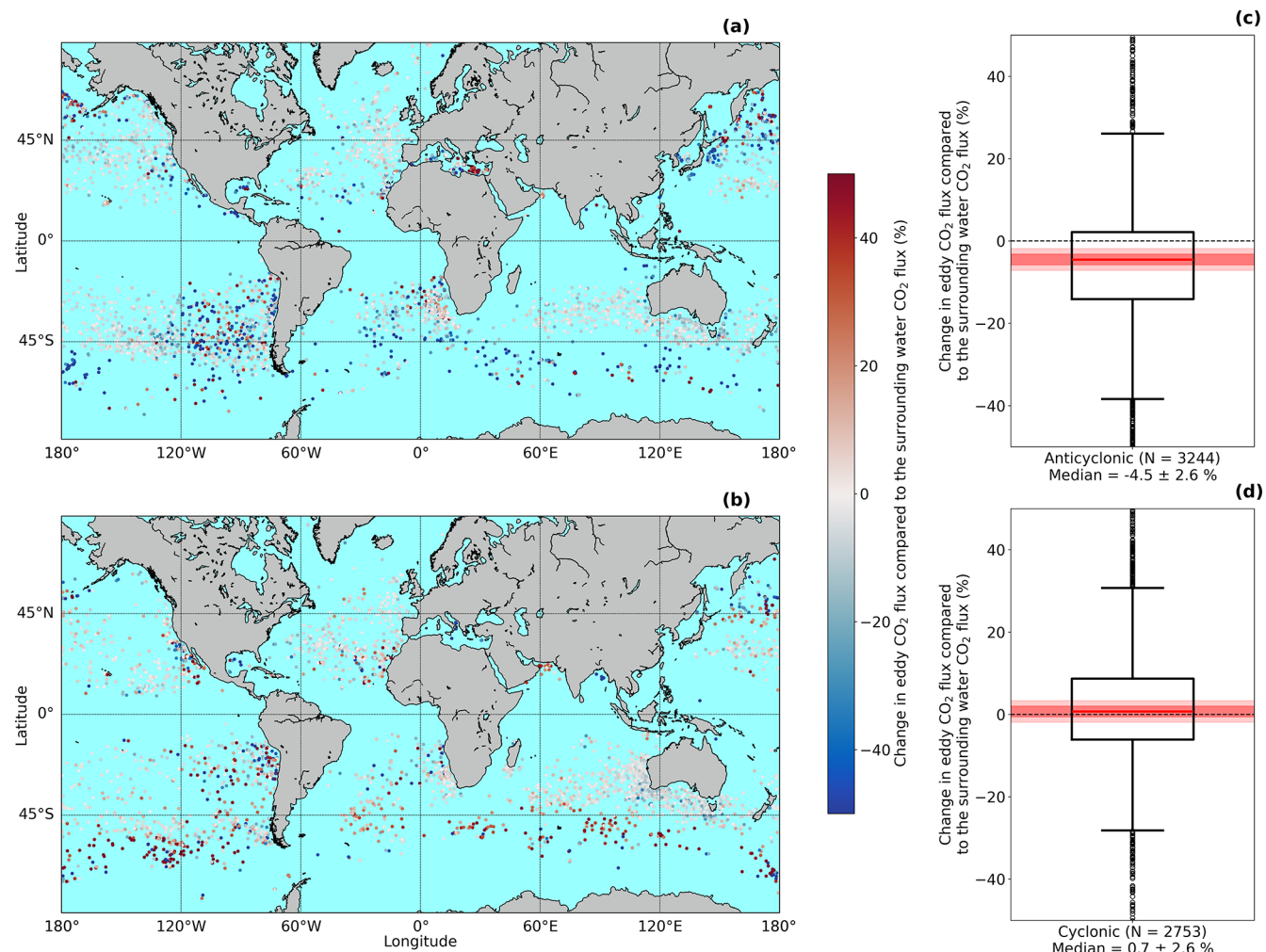


**Figure 7.** (a) Geographical distribution of the anticyclonic eddies' modification of the cumulative air-sea CO<sub>2</sub> flux. Negative values indicate a stronger CO<sub>2</sub> sink (weaker CO<sub>2</sub> source), and positive values indicate a weaker CO<sub>2</sub> sink (stronger CO<sub>2</sub> source). (b) Same as (a) for the cyclonic eddies. (c) Box plot showing the anticyclonic eddy modification of the air-sea CO<sub>2</sub> flux. Red line indicates the median, box indicates the 25th and 75th quartiles, whiskers extend from the 25th and 75th quartiles by 1.5 interquartile ranges. Circles indicate data considered outliers. Dark red shading indicates the 1 $\sigma$  (~68 % confidence) uncertainty on the median by propagating the air-sea CO<sub>2</sub> flux uncertainties using a Monte Carlo uncertainty propagation. Light red shading indicates the 2 $\sigma$  uncertainty on the median (~95 % confidence). X axis label shows number of eddies (N), the median modification with the 2 $\sigma$  uncertainty. (d) Same as (c) but for the cyclonic eddies. Basemap in (a) and (b) from Natural Earth v4.0.0 (<https://www.naturalearthdata.com/>, last access: 2 February 2025).

evaluated through time (e.g. Table S1 in the Supplement provides global decadal median mesoscale modifications suggesting an increasing enhancement of the CO<sub>2</sub> sink). Other potential applications could include, analysing the thermal and non-thermal components in driving the global eddy modified air-sea CO<sub>2</sub> fluxes (as illustrated by Ford et al. (2023) for the South Atlantic), or for investigating nutrient entrainment within the eddies and how it links to biological variations within the eddy track, or the variability in phytoplankton biomass and / or productivity within the eddies which are important for improving our understanding of carbon rate dynamics, and their impacts on ecology and biodiversity. The dataset presented here therefore provides the basis for a wide

range of studies to assess the evolution of mesoscale eddies and their air-sea CO<sub>2</sub> fluxes alongside understanding the linkages with their localised environmental conditions.

The air-sea CO<sub>2</sub> flux estimates are accompanied by a comprehensive uncertainty budget developed by Ford et al. (2024a) (Figs. 3 and 6). This is the first dataset of eddy air-sea CO<sub>2</sub> fluxes to include a uncertainty budget that has been built on the principles where all known sources of uncertainty are systematically considered (however small) and propagated to the final uncertainty using standard propagation techniques and a well-established uncertainty framework (BIPM, 2008; Taylor, 1997). The budget therefore provides an uncertainty on each air-sea CO<sub>2</sub> flux estimate, and

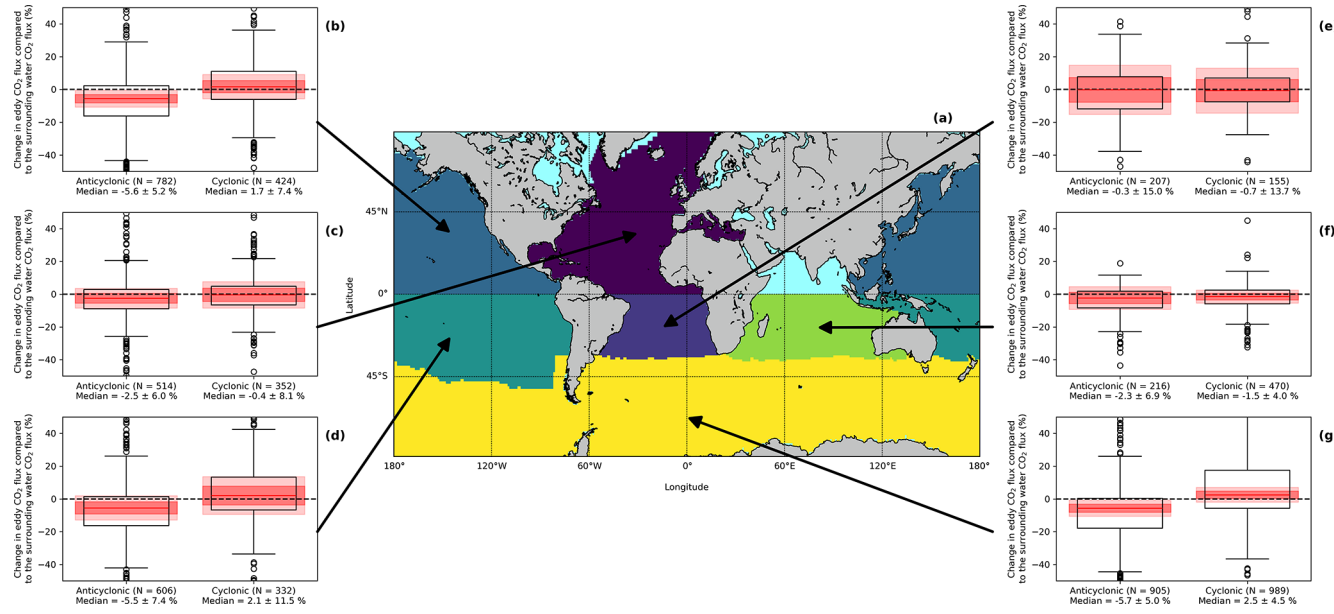


**Figure 8.** (a) Ocean basins considered for further analysis, with a colour for each region. Regions follow the RECCAP2 ocean basin definition, but each basin was split at the Equator into North and South. North Indian Ocean was removed due to low number of eddies analysed. (b) Box plot showing the eddy modification of the cumulative air-sea CO<sub>2</sub> flux for the region shown with the arrow. Red line indicates the median, box indicates the 25th and 75th quartiles, whiskers extend from the 25th and 75th quartiles by 1.5 interquartile ranges. Circles indicate data considered outliers (greater than 1.5 interquartile ranges outside the 25th and 75th percentile). Dark red shading indicates the 1 $\sigma$  (~68 % confidence) uncertainty on the median by propagating the air-sea CO<sub>2</sub> flux uncertainties using a Monte Carlo uncertainty propagation. Light red shading indicates the 2 $\sigma$  uncertainty on the median (~95 % confidence). X axis label shows number of eddy (N), the median modification with the 2 $\sigma$  uncertainty. (c–g) Same as (b) for their respective regions identified by the arrow. Basemap in (a) from Natural Earth v4.0.0 (<https://www.naturalearthdata.com/>, last access: 2 February 2025).

the  $f\text{CO}_{2(\text{sw})}$ , which can be accounted for within further analyses (e.g. as used in Ford et al., 2021, 2022b) and aids in assigning confidence to any results, as demonstrated in the example results that have been presented.

The comparisons between the UExP-FNN-U  $f\text{CO}_{2(\text{sw})}$  and SOCAT  $f\text{CO}_{2(\text{sw})}$  observations within eddies provide further confidence in the retrieved UExP-FNN-U  $f\text{CO}_{2(\text{sw})}$  and resulting air-sea CO<sub>2</sub> fluxes (Figs. 4 and 5). We showed that for both the anticyclonic and cyclonic eddies the within eddy accuracy (bias) and precision (RMSD) showed greater performance when compared to the global scale performance of these approaches (Ford et al., 2024a). This result was consistent with Ford et al. (2023) for the South Atlantic Ocean, who showed that both eddy types were well represented by the neural network approach (except that Ford et al., 2023 determined this from a lower number of crossover data points than presented here). Li et al. (2025) also showed for their neural network approach, similar accuracy and precision results for the  $f\text{CO}_{2(\text{sw})}$  within eddies for four western boundary current regions. Although, we did observe a slightly lower precision during the spring and summer, which could be due to the lack of a biological predictor (e.g. chl *a*) reducing the ability of the UExP-FNN-U to capture these dynamics (Ford et al., 2022a) (Fig. 5). These results also provide validity to the calculated  $f\text{CO}_{2(\text{sw})}$  uncertainties, which in

the majority of cases are dominated by the  $f\text{CO}_{2(\text{sw})}$  evaluation uncertainty component. As the retrieved within eddy  $f\text{CO}_{2(\text{sw})}$  bias and RMSD showed greater performance compared the global UExP-FNN-U performance (given in Ford et al., 2024a) we are confident in the UExP-FNN-U  $f\text{CO}_{2(\text{sw})}$  and uncertainty estimates within the eddies.

Within the UEx-L-Eddies we provide a secondary  $f\text{CO}_{2(\text{sw})}$  estimate (and associated air-sea CO<sub>2</sub> fluxes) from a global  $f\text{CO}_{2(\text{sw})}$  neural network, which included chl *a* as a predictor. We include the additional neural network because Ford et al. (2022a) highlighted that the inclusion of more representative biological parameters improved the regional estimation of  $f\text{CO}_{2(\text{sw})}$  in the South Atlantic Ocean, which is likely to be the same for other regions. Previous studies have shown the importance of biological modulation of  $f\text{CO}_{2(\text{sw})}$  within eddies (Orselli et al., 2019b), the resulting CO<sub>2</sub> fluxes, and how the importance changes over the eddy lifetime (Ford et al., 2023). This additional neural network showed similar but slightly improved precision (lower weighted RMSD) when compared to the in situ SOCAT observations, although to a lower number of data points (Fig. S2; anticyclonic bias = -0.92  $\mu\text{atm}$ , RMSD = 17.05  $\mu\text{atm}$ ,  $N$  = 1914; cyclonic bias = 0.05  $\mu\text{atm}$ , RMSD = 14.31  $\mu\text{atm}$ ,  $N$  = 1272). In addition, the seasonal breakdown of the comparisons between the within eddy UExP-FNN-U with chl *a*  $f\text{CO}_{2(\text{sw})}$

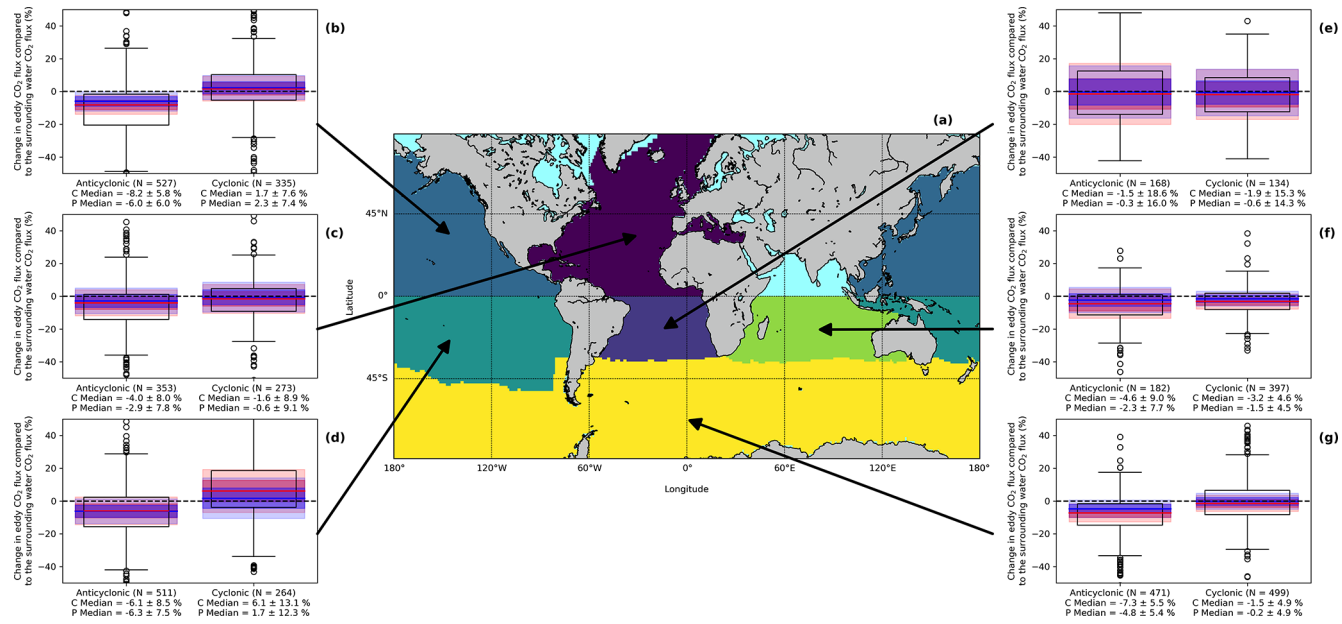


**Figure 9.** (a) Ocean basins considered for further analysis, with a colour for each region. Regions follow the RECCAP2 ocean basin definition, but each basin was split at the Equator into North and South. North Indian Ocean was removed due to low number of eddies analysed. (b) Box plot showing the eddy modification of the air-sea CO<sub>2</sub> flux using the chl *a* version of the UExP-FNN-U for the region shown with the arrow. Red line indicates the median, box indicates the 25th and 75th quartiles, whiskers extend from the 25th and 75th quartiles by 1.5 interquartile ranges. Circles indicate data considered outliers (greater than 1.5 interquartile ranges outside the 25th and 75th percentile). Dark red shading indicates the 1 $\sigma$  (~68 % confidence) uncertainty on the median by propagating the air-sea CO<sub>2</sub> flux uncertainties using a Monte Carlo uncertainty propagation. Light red shading indicates the 2 $\sigma$  uncertainty on the median (~95 % confidence). Blue line and shading indicates the same but for the UExP-FNN-U without chl *a*. *X* axis label shows number of eddy (*N*), the median modification with the 2 $\sigma$  uncertainty for the chl *a* version of the UExP-FNN-U labelled with a C, and the UExP-FNN-U without chl *a* labelled with a P. (c–g) Same as (b) for their respective regions identified by the arrow. Basemap in (a) from Natural Earth v4.0.0 (<https://www.naturalearthdata.com/>, last access: 2 February 2025).

and the in situ  $f\text{CO}_{2(\text{sw})}$  showed an increase in the performance of this neural network during spring and summer, highlighting the improvements from chl *a* being added as a predictor (Fig. S3). These estimates are however restricted to regions between 50°N and 50°S due to the availability of ocean colour chl *a* data in polar winter (i.e. for a full eddy timeseries the eddy must remain within the available ocean colour data).

The impact on the modification of the cumulative air-sea CO<sub>2</sub> flux by mesoscale eddies due to including chl *a* within the UExP-FNN-U can be assessed by replicating Fig. 8, but using the secondary  $f\text{CO}_{2(\text{sw})}$  and resulting air-sea CO<sub>2</sub> fluxes (Fig. 9). Figure 9 shows the regional modification of the air-sea CO<sub>2</sub> fluxes by eddies where both neural network variants are able to estimate the  $f\text{CO}_{2(\text{sw})}$  (i.e. we show a subset of the eddies in Fig. 8). In all regions both neural networks retrieve a similar signature, but the chl *a* version generally suggests a stronger enhancement (or weaker suppression) of the CO<sub>2</sub> sink compared to the UExP-FNN-U without chl *a*. Notably the South Pacific Ocean and Southern Ocean show larger differences although in all cases these differences fall within the uncertainties. We therefore provide

the secondary neural network to further aid in understanding the processes that are driving mesoscale eddy modification of the air-sea CO<sub>2</sub> fluxes.

Previous eddy trajectory datasets have been produced, for example Dong et al. (2022a), which include environmental datasets (e.g. SST) that can be used to understand the effects of eddies on physical and biological properties. The UEx-L-Eddies however extends the principles of these datasets to include air-sea CO<sub>2</sub> fluxes but also has a focus on climate quality dataset (i.e. the ESA CCI datasets) and provides comprehensive uncertainties. Therefore it provides a robust dataset for understanding long-lived eddy effects on the surface properties and air-sea CO<sub>2</sub> fluxes. In the future, we plan to include in situ observations by Biogeochemical Argo floats (BGC-Argo; Roemmich et al., 2019), which could be used to provide in situ based  $f\text{CO}_{2(\text{sw})}$  and air-sea CO<sub>2</sub> fluxes to further verify the air-sea CO<sub>2</sub> fluxes (e.g., as suggested by Keppler et al., 2024).

**Table 2.** Summary of methodologies in previous studies used to estimate the eddy modification of the air–sea  $\text{CO}_2$  flux.  $p\text{CO}_2(\text{sw})$  is the partial pressure of  $\text{CO}_2$  in seawater.

	This study	Guo and Timmermans (2024)	Li et al. (2025)	Keppler et al. (2024)	Ford et al. (2023)
Eddy dataset (or decomposition approach)	META 3.2	Mesoscale signature decomposition	META 3.2	META 3.2	META 3.1exp
Lifetimes considered	> 1 year	n/a	> 12 weeks	$\geq 10$ d	> 1 year
Radius threshold	No criteria	n/a	No criteria	> 40 km	No criteria
$f\text{CO}_2(\text{sw})$ estimation method	Global $f\text{CO}_2(\text{sw})$ neural network approach	Eddy resolving model	Regional $p\text{CO}_2(\text{sw})$ neural network approach	In situ pH with neural network Total Alkalinity	Regional $p\text{CO}_2(\text{sw})$ neural network approach
Temporal coverage	January 1993 to December 2022	1982 to 2000	July 2002 to 1 January 2022	April 2014 to February 2022	July 2002 to December 2018
Spatial Domain	Global	Global	Western Boundary Current (Kuroshio and Gulf Stream)	Southern Ocean	South Atlantic Ocean
Air sea $\text{CO}_2$ flux uncertainty treatment	Comprehensive uncertainty	n/a	$f\text{CO}_2(\text{sw})$ and gas transfer considered	Standard error of observations	$f\text{CO}_2(\text{sw})$ and gas transfer considered

n/a stands for not applicable.

#### 4.2 Comparison to previous global and regional eddy modifications of the air–sea $\text{CO}_2$ fluxes

Previous studies have investigated the effect of mesoscale eddies on global and regional air–sea  $\text{CO}_2$  fluxes (Table 2). Guo and Timmermans (2024) evaluate the cumulative effect of mesoscale variability on the air–sea  $\text{CO}_2$  flux globally, which they find enhances the global air–sea  $\text{CO}_2$  flux by  $0.72 \text{ Mt C yr}^{-1}$ , or  $0.72 \text{ Tg C yr}^{-1}$ . With the UEx-L-Eddies, if the individual eddy air–sea  $\text{CO}_2$  flux modifications are summed for the whole dataset, we find a global cumulative enhancement of the ocean  $\text{CO}_2$  sink by long-lived mesoscale eddies of  $75 \pm 33 \text{ Tg C}$  between 1993 and 2022. This would be equivalent to  $2.7 \pm 1.1 \text{ Tg C yr}^{-1}$  (95 % confidence interval). The calculated uncertainties with the UEx-L-Eddies allows robust uncertainty estimates to be provided alongside further analyses of the individual eddies, allowing significance of comparisons to be assessed. Differences here may be due to Guo and Timmermans (2024) including mesoscale variability not associated with mesoscale eddies (such as filaments, and current meanders), as their method does not track individual eddies. It could also be due to the UEx-L-Eddies only covering long-lived eddies, that represent 0.4 %

of eddies within the META3.2 trajectories dataset and therefore misses the contribution of smaller eddies (Pegliasco et al., 2022b) that would be included with Guo and Timmermans (2024).

Li et al. (2025) showed for the Kuroshio current that anticyclonic eddies enhanced the  $\text{CO}_2$  sink by  $15 \pm 1.73 \%$ , and cyclonic eddies reduced the  $\text{CO}_2$  sink by  $5.7 \pm 1.5 \%$ . Similar results were also shown for the Gulf Stream. Both the Gulf Stream and the Kuroshio current are dominated by short-lived eddies (e.g., those that survive for less than 1 year) in comparison to the long-lived eddies studied within the UEx-L-Eddies dataset, and therefore comparing these two estimates is inappropriate. However, our regional results for the North Pacific and North Atlantic Oceans do show a consistent direction of change (i.e., an enhanced sink) but with smaller magnitudes (Fig. 8).

Keppler et al. (2024) investigate the role of mesoscale eddies in modifying the air–sea  $\text{CO}_2$  flux in the Southern Ocean using Biogeochemical Argo profilers between April 2014 to December 2022. They find anticyclonic eddies enhanced the air–sea  $\text{CO}_2$  sink by  $7 \pm 2 \%$  and cyclonic eddies reduced the air–sea  $\text{CO}_2$  flux by  $2 \pm 2 \%$  ( $1\sigma$  uncertainties). Within the UEx-L-Eddies, we found that anticyclonic eddies en-

hanced the CO<sub>2</sub> sink by  $5.7 \pm 5.0\%$  ( $2\sigma$  uncertainties), and cyclonic eddies reduced the sink by  $2.5 \pm 4.5\%$  between 1993 and 2022 (Fig. 8g). These consistent results provide confidence to the air-sea CO<sub>2</sub> flux estimates within the UEx-L-Eddies.

Ford et al. (2023) showed that within the South Atlantic Ocean, anticyclonic ( $N = 36$ ) and cyclonic ( $N = 31$ ) eddies enhanced the CO<sub>2</sub> sink by 3.7% and 1.7%, respectively. In our analysis for the South Atlantic Ocean (Fig. 8e) we showed that anticyclonic enhanced the CO<sub>2</sub> sink by  $0.3 \pm 15.0\%$  ( $N = 207$ ) and cyclonic eddies enhanced the CO<sub>2</sub> sink by  $0.7 \pm 13.7\%$  ( $N = 155$ ) respectively, where confidence intervals are expressed as 95% confidence. Within this dataset, we consider  $\sim 5$  times more eddies than Ford et al. (2023) and find that the air-sea CO<sub>2</sub> flux uncertainties have a large effect on our resulting confidence, making the results indistinguishable at 95% confidence (even at 67% confidence the two are indistinguishable). The comparison highlights the importance of the calculated uncertainties and their use within further analyses and comparisons with other air-sea CO<sub>2</sub> fluxes.

The UEx-L-Eddies identifies differences in the mesoscale eddy modification of the cumulative air-sea CO<sub>2</sub> flux between anticyclonic and cyclonic eddies globally and regionally consistent with previous analyses. The driving mechanisms for these differences have been investigated in previous work. For example, Li et al. (2025) suggest that the competing changes in dissolved inorganic carbon and biological processes through eddy pumping contribute to the observed mesoscale eddy modification of the air-sea CO<sub>2</sub> flux. Additionally, Keppler et al. (2024) showed that the mesoscale modification of the air-sea CO<sub>2</sub> flux had significant seasonal variability in the Southern Ocean, indicating that underlying driving processes could vary throughout the individual eddies lifetime. Ford et al. (2023) showed that the changes in air-sea CO<sub>2</sub> flux in mesoscale eddies could be attributed to changes in the competing biological and physical processes. Although a comprehensive analysis of the driving mechanism is beyond the scope of this manuscript, the UEx-L-Eddies shows regional (Fig. 8) and seasonal variability in the mesoscale eddy modification of the air-sea CO<sub>2</sub> flux (e.g. Fig. S4 shows anticyclonic eddies have stronger uptake in winter). The underlying environmental parameters (e.g. SST, MLD) could therefore be used to investigate the driving mechanisms for these differences in the mesoscale modification.

#### 4.3 Limitations when using the UEx-L-Eddies

For some eddies the daily environmental data can have missing values even for complete coverage data (for example, the CCI-SST). These gaps stem from the META3.2 eddy trajectories dataset where the polygon to define the limits of the eddy does not form correctly, and therefore we were unable to extract values where the polygon was undefined. No exclu-

sion or interpolation mechanism was implemented as these data gaps affect a mean of 2% (maximum = 15%) of an individual eddy daily timeseries, which occur randomly through the timeseries, and therefore the impact on the monthly median statistics are minimal.

The UEx-L-Eddies dataset focusses on larger, long-lived eddies (lifetimes greater than a year). This criteria will regionally exclude eddies within, for example, highly dynamic western boundary currents where shorter lived eddies often dominate (Fig. 2c and d). Smith et al. (2023) however show that eddies with smaller radii generally have the same anomaly direction but with weaker magnitudes when compared to larger eddies. A previous study (Pegliasco et al., 2022b) identified that the shorter lived eddies within the Mesoscale Eddy Product (the same product used within this study) generally have smaller radii than the longer lived eddies. Therefore we would expect similar anomalies but of smaller magnitude when studying shorter lived eddies.

#### 5 Code and data availability

The code for the analysis is available, and version controlled on Github at <https://doi.org/10.5281/zenodo.18429374> (Ford et al., 2026). The UEx-L-Eddies dataset are available on Zenodo (<https://doi.org/10.5281/ZENODO.16355763>; Ford et al., 2025). The AVISO+ eddies trajectories data (META 3.2) was retrieved from AVISO+ (<https://doi.org/10.24400/527896/A01-2022.005.220209>; Pegliasco et al., 2022a). The CCI-SST climate record (v3.0) were retrieved from CEDA (<https://doi.org/10.5285/4A9654136A7148E39B7FEB56F8BB02D2>; Good and Embury, 2024). The OC-CCI chl-*a* (v6) were retrieved from CEDA (<https://doi.org/10.5285/5011D22AAE5A4671B0CBC7D05C56C4F0>; Sathyendranath et al., 2023). The CMEMS GLO-RYS12V1 SSS and MLD were retrieved from CMEMS (<https://doi.org/10.48670/moi-00021>; CMEMS, 2021). The CCMP wind speeds (v3.1) were retrieved from Remote Sensing Systems (<https://doi.org/10.56236/rss-uv6h30>; Remote Sensing Systems et al., 2022). The  $x\text{CO}_2(\text{atm})$  were retrieved from NOAA-GML (<https://doi.org/10.15138/DVNP-F961>; Lan et al., 2023). In situ SOCAT observations that have been recalculated to a consistent depth and temperature dataset were retrieved from Zenodo (<https://doi.org/10.5281/zenodo.15706025>; Ford et al., 2024d).

#### 6 Summary

The UEx-L-Eddies is a dataset of the air-sea CO<sub>2</sub> fluxes for ( $N = 5996$ ) long lived mesoscale eddies calculated in a Lagrangian mode within the global ocean. We use a global  $f\text{CO}_{2(\text{sw})}$  neural network (as used within one dataset submitted to the Global Carbon Budget called UExP-FNN-

U) to estimate the  $f\text{CO}_{2(\text{sw})}$  within the eddies at a monthly resolution. We prioritise the use of climate quality datasets within the analysis. The air-sea  $\text{CO}_2$  fluxes (also calculated following the methods of UExP-FNN-U) are accompanied by a comprehensive uncertainty budget (using a published methodology), that considers all known sources of uncertainty. We show for an exemplar eddy that the seasonal cycles of the eddy  $f\text{CO}_{2(\text{sw})}$  and air-sea  $\text{CO}_2$  fluxes are captured and can be cumulatively added to assess the  $\text{CO}_2$  uptake (or outgassing) of individual eddies. The comprehensive air-sea  $\text{CO}_2$  flux uncertainties provide a robust basis for assessing the confidence in the eddy air-sea  $\text{CO}_2$  flux estimates and can be propagated to further analysis. This illustrates how the importance of the different uncertainty components can change through time highlighting the shortfall of only quantifying selected contributions to the uncertainties or assuming fixed values.

Within the uncertainty assessment, we find that the  $f\text{CO}_{2(\text{sw})}$  in the eddies are estimated with an accuracy (bias) of  $-0.69 \mu\text{atm}$  and a precision (RMSD) of  $19.15 \mu\text{atm}$  for anticyclonic ( $N = 2082$ ), and accuracy of  $0.28 \mu\text{atm}$  and a precision of  $16.49 \mu\text{atm}$  for cyclonic eddies ( $N = 1376$ ). These accuracy and precision estimates provide validity to the neural network  $f\text{CO}_{2(\text{sw})}$ .

We demonstrate a use case of the UEx-L-Eddies dataset to evaluate the air-sea  $\text{CO}_2$  flux modification, and resultant integrated net  $\text{CO}_2$  sink, by long-lived mesoscale eddies, globally and regionally. We find that anticyclonic eddies enhance the net sink by  $4.5 \pm 2.8\%$  ( $N = 3244$ ), and cyclonic eddies suppress by  $0.7 \pm 2.6\%$  ( $N = 2752$ ) where uncertainties are the 95 % confidence interval. Regional differences in the eddy modification are observed, for example within the Southern Ocean, anticyclonic eddies enhanced the  $\text{CO}_2$  sink by  $5.7 \pm 5.0\%$ , and cyclonic eddies reduced the sink by  $2.5 \pm 4.5\%$ . We demonstrate how the use case results are consistent with previous regional analyses. Our example also highlighted the importance of using the accompanying uncertainty information when comparing studies, and caution should be taken in drawing conclusions from small samples or individual eddies, without considering the underlying comprehensive uncertainty budgets for the air-sea  $\text{CO}_2$  fluxes. The data presented could now be used to understand the processes occurring within these eddies that are driving these modifications of the air-sea  $\text{CO}_2$  fluxes, and how regionally these processes may vary.

**Supplement.** The supplement related to this article is available online at <https://doi.org/10.5194/essd-18-969-2026-supplement>.

**Author contributions.** DJF, GHT, VK, KS and JDS conceived the study and the methodology. DJF performed the analysis, testing of the dataset and wrote the original draft. All authors provided input to the final manuscript.

**Competing interests.** The contact author has declared that none of the authors has any competing interests.

**Disclaimer.** Publisher's note: Copernicus Publications remains neutral with regard to jurisdictional claims made in the text, published maps, institutional affiliations, or any other geographical representation in this paper. The authors bear the ultimate responsibility for providing appropriate place names. Views expressed in the text are those of the authors and do not necessarily reflect the views of the publisher.

**Acknowledgements.** Daniel J. Ford and Jamie D. Shutler were supported by funding from the European Space Agency under the projects “Satellite-based observations of Carbon in the Ocean: Pools, Fluxes and Exchanges” (SCOPE; 4000142532/23/I-DT) and ‘Ocean Carbon for Climate’ (OC4C; 3-18399/24/I-NB). Gavin H. Tilstone and Vassilis Kitidis were supported by The Atlantic Meridional Transect which is funded by the UK Natural Environment Research Council through its National Capability Long-term Single Centre Science Programme, Atlantic Climate and Environment Strategic Science –AtlantiS (grant number NE/Y005589/1). This study contributes to the international IM-BeR project and is contribution number 423 of the AMT programme.

The Surface Ocean  $\text{CO}_2$  Atlas (SOCAT) is an international effort, endorsed by the International Ocean Carbon Coordination Project (IOCCP), the Surface Ocean Lower Atmosphere Study (SOLAS) and the Integrated Marine Biosphere Research (IMBeR) program, to deliver a uniformly quality-controlled surface ocean  $\text{CO}_2$  database. The many researchers and funding agencies responsible for the collection of data and quality control are thanked for their contributions to SOCAT. For the purpose of open access, the authors have applied a Creative Commons Attribution (CC BY) licence to any Author Accepted Manuscript version arising from this submission.

**Financial support.** This research has been supported by the European Space Agency (grant nos. 4000142532/23/I-DT and 3-18399/24/I-NB) and the Natural Environment Research Council (grant no. NE/Y005589/1).

**Review statement.** This paper was edited by Xingchen (Tony) Wang and reviewed by Yiming Guo and one anonymous referee.

## References

Bakker, D. C. E., Pfeil, B., Landa, C. S., Metzl, N., O'Brien, K. M., Olsen, A., Smith, K., Cosca, C., Harasawa, S., Jones, S. D., Nakaoka, S. I., Nojiri, Y., Schuster, U., Steinhoff, T., Sweeney, C., Takahashi, T., Tilbrook, B., Wada, C., Wanninkhof, R., Alin, S. R., Balestrini, C. F., Barbero, L., Bates, N. R., Bianchi, A. A., Bonou, F., Boutin, J., Bozec, Y., Burger, E. F., Cai, W. J., Castle, R. D., Chen, L., Chierici, M., Currie, K., Evans, W., Featherstone, C., Feely, R. A., Fransson, A., Goyet, C., Greenwood, N., Gregor, L., Hankin, S., Hardman-Mountford, N. J., Harlay, J., Hauck, J., Hoppema, M., Humphreys, M. P., Hunt, C. W., Huss, B., Ibáñez, J. S. P., Johannessen, T., Keeling, R., Kitidis, V., Körtzinger, A., Kozyr, A., Krasakopoulou, E., Kuwata, A., Landschützer, P., Lauvset, S. K., Lefèvre, N., Lo Monaco, C., Manke, A., Mathis, J. T., Merlivat, L., Millero, F. J., Monteiro, P. M. S., Munro, D. R., Murata, A., Newberger, T., Omar, A. M., Ono, T., Paterson, K., Pearce, D., Pierrot, D., Robbins, L. L., Saito, S., Salisbury, J., Schlitzer, R., Schneider, B., Schweitzer, R., Sieger, R., Skjelvan, I., Sullivan, K. F., Sutherland, S. C., Sutton, A. J., Tadokoro, K., Telszewski, M., Tuma, M., Van Heuven, S. M. A. C., Vandemark, D., Ward, B., Watson, A. J., and Xu, S.: A multi-decade record of high-quality  $f\text{CO}_2$  data in version 3 of the Surface Ocean  $\text{CO}_2$  Atlas (SOCAT), *Earth Syst. Sci. Data*, 8, 383–413, <https://doi.org/10.5194/essd-8-383-2016>, 2016.

Bellenger, H., Bopp, L., Ethé, C., Ho, D., Duvel, J. P., Flavoni, S., Guez, L., Kataoka, T., Perrot, X., Parc, L., and Watanabe, M.: Sensitivity of the Global Ocean Carbon Sink to the Ocean Skin in a Climate Model, *J. Geophys. Res.-Oceans*, 128, e2022JC019479, <https://doi.org/10.1029/2022JC019479>, 2023.

BIPM: Evaluation of measurement data – Guide to the expression of uncertainty in measurement, <https://doi.org/10.59161/JCGM100-2008E>, 2008.

Chelton, D. B., Schlax, M. G., and Samelson, R. M.: Global observations of nonlinear mesoscale eddies, *Prog. Oceanogr.*, 91, 167–216, <https://doi.org/10.1016/j.pocean.2011.01.002>, 2011.

Chen, F., Cai, W. J., Benitez-Nelson, C., and Wang, Y.: Sea surface  $p\text{CO}_2$ -SST relationships across a cold-core cyclonic eddy: Implications for understanding regional variability and air-sea gas exchange, *Geophys. Res. Lett.*, 34, <https://doi.org/10.1029/2006GL028058>, 2007.

CMEMS: Copernicus Marine Modelling Service global ocean physics reanalysis product (GLORYS12V1), Copernicus Marine Modelling Service [data set], <https://doi.org/10.48670/moi-00021>, 2021.

Dickson, A. G., Sabine, C. L., and Christian, J. R.: Guide to Best Practices for Ocean  $\text{CO}_2$  measurements, PICES Special Publication, IOC Report No. 8, North Pacific Marine Science Organization, ISBN 1-897176-07-4, 2007.

Dong, C., Liu, L., Nencioli, F., Bethel, B. J., Liu, Y., Xu, G., Ma, J., Ji, J., Sun, W., Shan, H., Lin, X., and Zou, B.: The near-global ocean mesoscale eddy atmospheric-oceanic-biological interaction observational dataset, *Sci. Data*, 9, 436, <https://doi.org/10.1038/s41597-022-01550-9>, 2022a.

Dong, Y., Bakker, D. C. E., Bell, T. G., Huang, B., Landschützer, P., Liss, P. S., and Yang, M.: Update on the Temperature Corrections of Global Air-Sea  $\text{CO}_2$  Flux Estimates, *Global Biogeoch. Cy.*, 36, <https://doi.org/10.1029/2022GB007360>, 2022b.

Dong, Y., Bakker, D. C. E., Bell, T. G., Yang, M., Landschützer, P., Hauck, J., Rödenbeck, C., Kitidis, V., Bushinsky, S. M., and Liss, P. S.: Direct observational evidence of strong  $\text{CO}_2$  uptake in the Southern Ocean, *Sci. Adv.*, 10, eadn5781, <https://doi.org/10.1126/sciadv.adn5781>, 2024.

Donlon, C. J., Nightingale, T. J., Sheasby, T., Turner, J., Robinson, I. S., and Emery, W. J.: Implications of the oceanic thermal skin temperature deviation at high wind speed, *Geophys. Res. Lett.*, 26, 2505–2508, <https://doi.org/10.1029/1999GL900547>, 1999.

Dufois, F., Hardman-Mountford, N. J., Greenwood, J., Richardson, A. J., Feng, M., and Matear, R. J.: Anticyclonic eddies are more productive than cyclonic eddies in subtropical gyres because of winter mixing, *Sci. Adv.*, 2, 1–7, <https://doi.org/10.1126/sciadv.1600282>, 2016.

Embury, O.: SST CCI Product Validation and Intercomparison Report, [https://climate.esa.int/documents/2369/SST\\_CCI\\_D4.1\\_PVIR\\_v2.1-signed.pdf](https://climate.esa.int/documents/2369/SST_CCI_D4.1_PVIR_v2.1-signed.pdf) (last access: 2 March 2025), 2023.

Embury, O., Merchant, C. J., Good, S. A., Rayner, N. A., Høyér, J. L., Atkinson, C., Block, T., Alerskans, E., Pearson, K. J., Worsfold, M., McCarroll, N., and Donlon, C.: Satellite-based time-series of sea-surface temperature since 1980 for climate applications, *Sci. Data*, 11, 326, <https://doi.org/10.1038/s41597-024-03147-w>, 2024.

Fairall, C. W., Bradley, E. F., Godfrey, J. S., Wick, G. A., Edson, J. B., and Young, G. S.: Cool-skin and warm-layer effects on sea surface temperature, *J. Geophys. Res.-Oceans*, 101, 1295–1308, <https://doi.org/10.1029/95JC03190>, 1996.

Ford, D. J., Tilstone, G. H., Shutler, J. D., Kitidis, V., Lobanova, P., Schwarz, J., Poulton, A. J., Serret, P., Lamont, T., Chuqui, M., Barlow, R., Lozano, J., Kampel, M., and Brandini, F.: Wind speed and mesoscale features drive net autotrophy in the South Atlantic Ocean, *Remote Sens. Environ.*, 260, 112435, <https://doi.org/10.1016/j.rse.2021.112435>, 2021.

Ford, D. J., Tilstone, G. H., Shutler, J. D., and Kitidis, V.: Derivation of seawater  $p\text{CO}_2$  from net community production identifies the South Atlantic Ocean as a  $\text{CO}_2$  source, *Biogeosciences*, 19, 93–115, <https://doi.org/10.5194/bg-19-93-2022>, 2022a.

Ford, D. J., Tilstone, G. H., Shutler, J. D., and Kitidis, V.: Identifying the biological control of the annual and multi-year variations in South Atlantic air-sea  $\text{CO}_2$  flux, *Biogeosciences*, 19, 4287–4304, <https://doi.org/10.5194/bg-19-4287-2022>, 2022b.

Ford, D. J., Tilstone, G. H., Shutler, J. D., Kitidis, V., Sheen, K. L., Dall'Olmo, G., and Orselli, I. B. M.: Mesoscale Eddies Enhance the Air-Sea  $\text{CO}_2$  Sink in the South Atlantic Ocean, *Geophys. Res. Lett.*, 50, e2022GL102137, <https://doi.org/10.1029/2022GL102137>, 2023.

Ford, D. J., Blannin, J., Watts, J., Watson, A. J., Landschützer, P., Jersild, A., and Shutler, J. D.: A Comprehensive Analysis of Air-Sea  $\text{CO}_2$  Flux Uncertainties Constructed From Surface Ocean Data Products, *Global Biogeochem. Cy.*, 38, e2024GB008188, <https://doi.org/10.1029/2024GB008188>, 2024a.

Ford, D. J., Shutler, J. D., Blanco-Sacristán, J., Corrigan, S., Bell, T. G., Yang, M., Kitidis, V., Nightingale, P. D., Brown, I., Wimmer, W., Woolf, D. K., Casal, T., Donlon, C., Tilstone, G. H., and Ashton, I.: Enhanced ocean  $\text{CO}_2$  uptake due to near-surface temperature gradients, *Nat. Geosci.*, 17, 1135–1140, <https://doi.org/10.1038/s41561-024-01570-7>, 2024b.

Ford, D. J., Blannin, J., Watts, J., Watson, A. J., Landschützer, P., Jersild, A., and Shutler, J. D.: OceanICU Neural Network

Framework with per pixel uncertainty propagation (v1.1), Zenodo [code], <https://doi.org/10.5281/ZENODO.12597803>, 2024c.

Ford, D. J., Shutler, J. D., Ashton, I., Sims, R. P., and Holding, T.: Reanalysed (depth and temperature consistent) Surface Ocean CO<sub>2</sub> Atlas (SOCAT) version 2024 (v1.1), Zenodo [data set], <https://doi.org/10.5281/ZENODO.13284017>, 2024d.

Ford, D. J., Shutler, J. D., Sheen, K. L., Tilstone, G. H., and Kitidis, V.: UEx-L-Eddies: decadal and global long-lived mesoscale eddy trajectories with coincident air-sea CO<sub>2</sub> fluxes and biogeochemical conditions (v0-2), Zenodo [data set], <https://doi.org/10.5281/ZENODO.16355763>, 2025.

Ford, D. J., Shutler, J. D., Sheen, K. L., Tilstone, G. H., and Vassilis, K.: pyEddyCO2: Python code to extract biogeochemical properties for mesoscale eddies (Version v1), Zenodo [code], <https://doi.org/10.5281/zenodo.18429374>, 2026.

Frenger, I., Gruber, N., Knutti, R., and Münnich, M.: Imprint of Southern Ocean eddies on winds, clouds and rainfall, *Nat. Geosci.*, 6, 608–612, <https://doi.org/10.1038/ngeo1863>, 2013.

Friedlingstein, P., O’Sullivan, M., Jones, M. W., Andrew, R. M., Hauck, J., Landschützer, P., Le Quéré, C., Li, H., Luijckx, I. T., Olsen, A., Peters, G. P., Peters, W., Pongratz, J., Schwingshakel, C., Sitch, S., Canadell, J. G., Ciais, P., Jackson, R. B., Alin, S. R., Arneth, A., Arora, V., Bates, N. R., Becker, M., Bellouin, N., Berghoff, C. F., Bittig, H. C., Bopp, L., Cadule, P., Campbell, K., Chamberlain, M. A., Chandra, N., Chevallier, F., Chini, L. P., Colligan, T., Decayeux, J., Djeutchouang, L. M., Dou, X., Duran Rojas, C., Enyo, K., Evans, W., Fay, A. R., Feely, R. A., Ford, D. J., Foster, A., Gasser, T., Gehlen, M., Gkritzalis, T., Grassi, G., Gregor, L., Gruber, N., Gürses, Ö., Harris, I., Hefner, M., Heinke, J., Hurt, G. C., Iida, Y., Ilyina, T., Jacobson, A. R., Jain, A. K., Jarníková, T., Jersild, A., Jiang, F., Jin, Z., Kato, E., Keeling, R. F., Klein Goldewijk, K., Knauer, J., Korsbakken, J. I., Lan, X., Lauvset, S. K., Lefèvre, N., Liu, Z., Liu, J., Ma, L., Maksyutov, S., Marland, G., Mayot, N., McGuire, P. C., Metzl, N., Monacci, N. M., Morgan, E. J., Nakaoka, S.-I., Neill, C., Niwa, Y., Nützel, T., Olivier, L., Ono, T., Palmer, P. I., Pierrot, D., Qin, Z., Resplandy, L., Roobaert, A., Rosan, T. M., Rödenbeck, C., Schwinger, J., Smallman, T. L., Smith, S. M., Sospedra-Alfonso, R., Steinhoff, T., Sun, Q., Sutton, A. J., Séférian, R., Takao, S., Tatebe, H., Tian, H., Tilbrook, B., Torres, O., Tourigny, E., Tsujino, H., Tubiello, F., van der Werf, G., Wanninkhof, R., Wang, X., Yang, D., Yang, X., Yu, Z., Yuan, W., Yue, X., Zaehle, S., Zeng, N., and Zeng, J.: Global Carbon Budget 2024, *Earth Syst. Sci. Data*, 17, 965–1039, <https://doi.org/10.5194/essd-17-965-2025>, 2025.

Goddijn-Murphy, L. M., Woolf, D. K., Land, P. E., Shutler, J. D., and Donlon, C.: The OceanFlux Greenhouse Gases methodology for deriving a sea surface climatology of CO<sub>2</sub> fugacity in support of air-sea gas flux studies, *Ocean Sci.*, 11, 519–541, <https://doi.org/10.5194/os-11-519-2015>, 2015.

Good, S. A. and Embury, O.: ESA Sea Surface Temperature Climate Change Initiative (SST\_cci): Level 4 Analysis product, version 3.0, CEDA Archive [data set], <https://doi.org/10.5285/4A9654136A7148E39B7FEB56F8BB02D2>, 2024.

Guo, Y. and Timmermans, M.: The Role of Ocean Mesoscale Variability in Air-Sea CO<sub>2</sub> Exchange: A Global Perspective, *Geophys. Res. Lett.*, 51, e2024GL108373, <https://doi.org/10.1029/2024GL108373>, 2024.

Hersbach, H., Bell, B., Berrisford, P., Biavati, G., Horányi, A., Muñoz Sabater, J., Nicolas, J., Peubey, C., Radu, R., Rozum, I., Schepers, D., Simmons, A., Soci, C., Dee, D., and Thépaut, J.-N.: ERA5 monthly averaged data on single levels from 1979 to present, Copernicus Climate Change Service (C3S) Climate Data Store (CDS) [data set], <https://doi.org/10.24381/cds.f17050d7>, 2019.

Hersbach, H., Bell, B., Berrisford, P., Hirahara, S., Horányi, A., Muñoz-Sabater, J., Nicolas, J., Peubey, C., Radu, R., Schepers, D., Simmons, A., Soci, C., Abdalla, S., Abellan, X., Balsamo, G., Bechtold, P., Biavati, G., Bidlot, J., Bonavita, M., Chiara, G., Dahlgren, P., Dee, D., Diamantakis, M., Dragani, R., Flemming, J., Forbes, R., Fuentes, M., Geer, A., Haimberger, L., Healy, S., Hogan, R. J., Hólm, E., Janisková, M., Keeley, S., Laloyaux, P., Lopez, P., Lupu, C., Radnoti, G., Rosnay, P., Rozum, I., Vamborg, F., Villaume, S., and Thépaut, J.: The ERA5 global reanalysis, *Q. J. Roy. Meteorol. Soc.*, 146, 1999–2049, <https://doi.org/10.1002/qj.3803>, 2020.

Holding, T., Ashton, I. G., Shutler, J. D., Land, P. E., Nightingale, P. D., Rees, A. P., Brown, I., Piolle, J.-F., Kock, A., Bange, H. W., Woolf, D. K., Goddijn-Murphy, L., Pereira, R., Paul, F., Girard-Ardhuin, F., Chapron, B., Rehder, G., Ardhuin, F., and Donlon, C. J.: The FluxEngine air-sea gas flux toolbox: simplified interface and extensions for in situ analyses and multiple sparingly soluble gases, *Ocean Sci.*, 15, 1707–1728, <https://doi.org/10.5194/os-15-1707-2019>, 2019.

Jean-Michel, L., Eric, G., Romain, B.-B., Gilles, G., Angélique, M., Marie, D., Clément, B., Mathieu, H., Olivier, L. G., Charly, R., Tony, C., Charles-Emmanuel, T., Florent, G., Giovanni, R., Mounir, B., Yann, D., and Pierre-Yves, L. T.: The Copernicus Global 1/12° Oceanic and Sea Ice GLORYS12 Reanalysis, *Front. Earth Sci.*, 9, 1–27, <https://doi.org/10.3389/feart.2021.698876>, 2021.

Jones, E. M., Hoppema, M., Strass, V., Hauck, J., Salt, L., Ossebaar, S., Klaas, C., van Heuven, S. M. A. C., Wolf-Gladrow, D., Stöven, T., and de Baar, H. J. W.: Mesoscale features create hotspots of carbon uptake in the Antarctic Circumpolar Current, *Deep-Sea Res. Pt. II*, 138, 39–51, <https://doi.org/10.1016/j.dsr2.2015.10.006>, 2017.

Keppler, L., Eddebar, Y. A., Gille, S. T., Guisewhite, N., Mazloff, M. R., Tamsitt, V., Verdy, A., and Talley, L. D.: Effects of Mesoscale Eddies on Southern Ocean Biogeochemistry, *AGU Adv.*, 5, e2024AV001355, <https://doi.org/10.1029/2024AV001355>, 2024.

Lan, X., Tans, P., Thoning, K., and NOAA Global Monitoring Laboratory: NOAA Greenhouse Gas Marine Boundary Layer Reference – CO<sub>2</sub>, NOAA [data set], <https://doi.org/10.15138/DVNP-F961>, 2023.

Laws, E. A.: Mathematical methods for oceanographers: an introduction, Wiley, New York, 343 pp., ISBN 978-0-471-16221-6, 1997.

Laxenaire, R., Speich, S., and Stegner, A.: Evolution of the Thermo-haline Structure of One Agulhas Ring Reconstructed from Satellite Altimetry and Argo Floats, *J. Geophys. Res.-Oceans*, 124, 8969–9003, <https://doi.org/10.1029/2018JC014426>, 2019.

Li, X., Gan, B., Zhang, Z., Cao, Z., Qiu, B., Chen, Z., and Wu, L.: Oceanic uptake of CO<sub>2</sub> enhanced by mesoscale eddies, *Sci. Adv.*, 11, eadtf4195, <https://doi.org/10.1126/sciadv.adt4195>, 2025.

Mears, C., Lee, T., Ricciardulli, L., Wang, X., and Wentz, F.: Improving the Accuracy of the Cross-Calibrated Multi-

Platform (CCMP) Ocean Vector Winds, *Remote Sens.*, 14, 4230, <https://doi.org/10.3390/rs14174230>, 2022.

Nencioli, F., Dall'Olmo, G., and Quartly, G. D.: Agulhas Ring Transport Efficiency From Combined Satellite Altimetry and Argo Profiles, *J. Geophys. Res.-Oceans*, 123, 5874–5888, <https://doi.org/10.1029/2018JC013909>, 2018.

Nightingale, P. D., Malin, G., Law, C. S., Watson, A. J., Liss, P. S., Liddicoat, M. I., Boutin, J., and Upstill-Goddard, R. C.: In situ evaluation of air-sea gas exchange parameterizations using novel conservative and volatile tracers, *Global Biogeochem. Cy.*, 14, 373–387, <https://doi.org/10.1029/1999GB900091>, 2000.

Orselli, I. B. M., Goyet, C., Kerr, R., de Azevedo, J. L. L., Araujo, M., Galdino, F., Touratier, F., and Garcia, C. A. E.: The effect of Agulhas eddies on absorption and transport of anthropogenic carbon in the South Atlantic Ocean, *Climate*, 7, 1–25, <https://doi.org/10.3390/CLI7060084>, 2019a.

Orselli, I. B. M., Kerr, R., de Azevedo, J. L. L., Galdino, F., Araujo, M., and Garcia, C. A. E.: The sea-air CO<sub>2</sub> net fluxes in the South Atlantic Ocean and the role played by Agulhas eddies, *Prog. Oceanogr.*, 170, 40–52, <https://doi.org/10.1016/j.pocean.2018.10.006>, 2019b.

Pegliasco, C., Busche, C., and Faugere, Y.: Mesoscale Eddy Trajectory Atlas META3.2 Delayed-Time all satellites: version META3.2 DT allsat (3.2 DT allsat 1993-01-01/2022-02-09), AVISO+ [data set], <https://doi.org/10.24400/527896/A01-2022.005.220209>, 2022a.

Pegliasco, C., Delepouille, A., Mason, E., Morrow, R., Faugère, Y., and Dibarboure, G.: META3.1exp: a new global mesoscale eddy trajectory atlas derived from altimetry, *Earth Syst. Sci. Data*, 14, 1087–1107, <https://doi.org/10.5194/essd-14-1087-2022>, 2022b.

Pezzi, L. P., de Souza, R. B., Santini, M. F., Miller, A. J., Carvalho, J. T., Parise, C. K., Quadro, M. F., Rosa, E. B., Justino, F., Sutil, U. A., Cabrera, M. J., Babanin, A. V., Voermans, J., Nascimento, E. L., Alves, R. C. M., Munchow, G. B., and Rubert, J.: Oceanic eddy-induced modifications to air-sea heat and CO<sub>2</sub> fluxes in the Brazil-Malvinas Confluence, *Sci. Rep.*, 11, 10648, <https://doi.org/10.1038/s41598-021-89985-9>, 2021.

Remote Sensing Systems, Mears, C., Lee, T., Ricciardulli, L., Wang, X., and Wentz, F.: RSS Cross-Calibrated Multi-Platform (CCMP) 6-hourly ocean vector wind analysis on 0.25 deg grid, Version 3.0, Remote Sensing Systems [data set], <https://doi.org/10.56236/rss-uv6h30>, 2022.

Roemmich, D., Alford, M. H., Claustre, H., Johnson, K. S., King, B., Moum, J., Oke, P. R., Owens, W. B., Pouliquen, S., Purkey, S., Scanderbeg, M., Suga, T., Wijffels, S. E., Zilberman, N., Bakker, D., Baringer, M. O., Belbeoch, M., Bittig, H. C., Boss, E., Calil, P., Carse, F., Carval, T., Chai, F., Conchubhair, D. O., D'Ortenzio, F., Dall'Olmo, G., Desbruyères, D., Fennel, K., Fer, I., Ferrari, R., Forget, G., Freeland, H., Fujiki, T., Gehlen, M., Greenan, B., Hallberg, R., Hibiya, T., Hosoda, S., Jayne, S., Jochum, M., Johnson, G. C., Kang, K. R., Kolodziejczyk, N., Koertzinger, A., Le Traon, P. Y., Lenn, Y. D., Maze, G., Mork, K. A., Morris, T., Nagai, T., Nash, J., Garabato, A. N., Olsen, A., Pattabhi, R. R., Prakash, S., Riser, S., Schmechtig, C., Shroyer, E., Sterl, A., Sutton, P., Talley, L., Tanhua, T., Thierry, V., Thomalla, S., Too, J., Troisi, A., Trull, T., Tutton, J. D., Velez-Belchi, P. J., Walczowski, W., Wang, H., Wanninkhof, R., Waterhouse, A., Watson, A., Wilson, C., Wong, A. P., Xu, J., and Yasuda, I.: On the future of Argo: A global, full-depth, multi-disciplinary array, *Front. Mar. Sci.*, 6, 1–28, <https://doi.org/10.3389/fmars.2019.00439>, 2019.

Sathyendranath, S., Brewin, R. J. W., Brockmann, C., Brotas, V., Calton, B., Chuprin, A., Cipollini, P., Couto, A. B., Dingle, J., Doerffer, R., Donlon, C., Dowell, M., Farman, A., Grant, M., Groom, S., Horsman, A., Jackson, T., Krasemann, H., Lavender, S., Martinez-Vicente, V., Mazeran, C., Mélin, F., Moore, T. S., Müller, D., Regner, P., Roy, S., Steele, C. J., Steinmetz, F., Swinton, J., Taberner, M., Thompson, A., Valente, A., Zühlke, M., Brando, V. E., Feng, H., Feldman, G., Franz, B. A., Frouin, R., Gould, R. W., Hooker, S. B., Kahru, M., Kratzer, S., Mitchell, B. G., Muller-Karger, F. E., Sosik, H. M., Voss, K. J., Werdell, J., and Platt, T.: An ocean-colour time series for use in climate studies: The experience of the ocean-colour climate change initiative (OC-CCI), *Sensors*, 19, <https://doi.org/10.3390/s19194285>, 2019.

Sathyendranath, S., Jackson, T., Brockmann, C., Brotas, V., Calton, B., Chuprin, A., Clements, O., Cipollini, P., Danne, O., Dingle, J., Donlon, C., Grant, M., Groom, S., Krasemann, H., Lavender, S., Mazeran, C., Mélin, F., Müller, D., Steinmetz, F., Valente, A., Zühlke, M., Feldman, G., Franz, B., Frouin, R., Werdell, J., and Platt, T.: ESA Ocean Colour Climate Change Initiative (Ocean\_Colour\_cci): Version 6.0, 4 km resolution data, CEDA Archive [data set], <https://doi.org/10.5285/5011D22AAE5A4671B0CBC7D05C56C4F0>, 2023.

Shutler, J. D., Land, P. E., Piole, J. F., Woolf, D. K., Goddijn-Murphy, L., Paul, F., Girard-Ardhuin, F., Chapron, B., and Donlon, C. J.: FluxEngine: A flexible processing system for calculating atmosphere-ocean carbon dioxide gas fluxes and climatologies, *J. Atmos. Ocean. Tech.*, 33, 741–756, <https://doi.org/10.1175/JTECH-D-14-00204.1>, 2016.

Shutler, J. D., Wanninkhof, R., Nightingale, P. D., Woolf, D. K., Bakker, D. C., Watson, A., Ashton, I., Holding, T., Chapron, B., Quilfen, Y., Fairall, C., Schuster, U., Nakajima, M., and Donlon, C. J.: Satellites will address critical science priorities for quantifying ocean carbon, *Front. Ecol. Environ.*, 18, 27–35, <https://doi.org/10.1002/fee.2129>, 2020.

Shutler, J. D., Gruber, N., Findlay, H. S., Land, P. E., Gregor, L., Holding, T., Sims, R. P., Green, H., Piole, J.-F., Chapron, B., Sathyendranath, S., Rousseaux, C. S., Donlon, C. J., Cooley, S., Turner, J., Valauri-Orton, A., Lowder, K., Widdicombe, S., Newton, J., Sabia, R., Rio, M.-H., and Gaultier, L.: The increasing importance of satellite observations to assess the ocean carbon sink and ocean acidification, *Earth-Sci. Rev.*, 250, 104682, <https://doi.org/10.1016/j.earscirev.2024.104682>, 2024.

Smith, T. G., Nicholson, S.-A., Engelbrecht, F. A., Chang, N., Mongwe, N. P., and Monteiro, P. M. S.: The Heat and Carbon Characteristics of Modeled Mesoscale Eddies in the South-East Atlantic Ocean, *J. Geophys. Res.-Oceans*, 128, e2023JC020337, <https://doi.org/10.1029/2023JC020337>, 2023.

Song, H., Marshall, J., Munro, D. R., Dutkiewicz, S., Sweeney, C., McGillicuddy, D. J., and Hausmann, U.: Mesoscale modulation of air-sea CO<sub>2</sub> flux in Drake Passage, *J. Geophys. Res.-Oceans*, 121, 6635–6649, <https://doi.org/10.1002/2016JC011714>, 2016.

Taylor, J. R.: An introduction to error analysis, University Science Books, Sausalito, California, ISBN 9780935702750, 1997.

Watson, A. J., Schuster, U., Shutler, J. D., Holding, T., Ashton, I. G. C., Landschützer, P., Woolf, D. K., and Goddijn-Murphy, L.: Revised estimates of ocean-atmosphere CO<sub>2</sub> flux are con-

sistent with ocean carbon inventory, *Nat. Commun.*, 11, 1–6, <https://doi.org/10.1038/s41467-020-18203-3>, 2020.

Weiss, R. F.: Carbon dioxide in water and seawater: the solubility of a non-ideal gas, *Mar. Chem.*, 2, 203–215, [https://doi.org/10.1016/0304-4203\(74\)90015-2](https://doi.org/10.1016/0304-4203(74)90015-2), 1974.

Woolf, D. K., Land, P. E., Shutler, J. D., Goddijn-Murphy, L. M., and Donlon, C. J.: On the calculation of air-sea fluxes of CO<sub>2</sub> in the presence of temperature and salinity gradients, *J. Geophys. Res.-Oceans*, 121, 1229–1248, <https://doi.org/10.1002/2015JC011427>, 2016.

Woolf, D. K., Shutler, J. D., Goddijn-Murphy, L., Watson, A. J., Chapron, B., Nightingale, P. D., Donlon, C. J., Piskozub, J., Yelland, M. J., Ashton, I., Holding, T., Schuster, U., Girard-Ardhuin, F., Grouazel, A., Piolle, J. F., Warren, M., Wrobel-Niedzwiecka, I., Land, P. E., Torres, R., Prytherch, J., Moat, B., Hanafin, J., Ardhuin, F., and Paul, F.: Key Uncertainties in the Recent Air-Sea Flux of CO<sub>2</sub>, *Global Biogeochem. Cy.*, 33, 1548–1563, <https://doi.org/10.1029/2018GB006041>, 2019.

York, D., Evensen, N. M., Martínez, M. L., and De Basabe Delgado, J.: Unified equations for the slope, intercept, and standard errors of the best straight line, *Am. J. Phys.*, 72, 367–375, <https://doi.org/10.1119/1.1632486>, 2004.